



## Evaluating the sensitivity of radical chemistry and ozone formation to ambient VOCs and NO<sub>x</sub> in Beijing

Lisa K. Whalley<sup>1,2</sup>, Eloise J. Slater<sup>1</sup>, Robert Woodward-Massey<sup>1,a</sup>, Chunxiang Ye<sup>1,a</sup>, James D Lee<sup>3,4</sup>,  
5 Freya Squires<sup>4</sup>, James R. Hopkins<sup>3,4</sup>, Rachel E Dunmore<sup>4</sup>, Marvin Shaw<sup>3,4</sup>, Jacqueline F. Hamilton<sup>4</sup>,  
Alastair C Lewis<sup>3,4</sup>, Archit Mehra<sup>5,b</sup>, Stephen D. Worrall<sup>5,c</sup>, Asan Bacak<sup>5,d</sup>, Thomas J. Bannan<sup>5</sup>, Hugh  
Coe<sup>5,6</sup>, Bin Ouyang<sup>7,e</sup>, Roderic L. Jones<sup>7</sup>, Leigh R. Crilley<sup>8,f</sup>, Louisa J. Kramer<sup>8</sup>, William J. Bloss<sup>8</sup>, Tuan  
Vu<sup>8</sup>, Simone Kotthaus<sup>9,10</sup>, Sue Grimmond<sup>9</sup>, Yele Sun<sup>11</sup>, Weiqi Xu<sup>11</sup>, Siyao Yue<sup>11</sup>, Lujie Ren<sup>11</sup>, W. Joe F.  
Acton<sup>12</sup>, C. Nicholas Hewitt<sup>12</sup>, Xinming Wang<sup>13</sup>, Pingqing Fu<sup>14</sup> and Dwayne E. Heard<sup>1</sup>

10

<sup>1</sup>School of Chemistry, University of Leeds, Leeds, LS2 9JT, UK

<sup>2</sup>National Centre for Atmospheric Science, University of Leeds, Leeds, LS2 9JT, UK

<sup>3</sup>National Centre for Atmospheric Science, University of York, Heslington, York, YO10 5DD, UK

<sup>4</sup>Wolfson Atmospheric Chemistry Laboratories, Department of Chemistry, University of York, Heslington, York, 10 YO10  
15 5DD, UK

<sup>5</sup>Centre for Atmospheric Science, School of Earth and Environmental Sciences, The University of Manchester, Manchester,  
M13 9PL, UK

<sup>6</sup>National Centre for Atmospheric Science, University of Manchester, Manchester, M13 9PL, UK

<sup>7</sup>Department of Chemistry, University of Cambridge, UK

20 <sup>8</sup>School of Geography, Earth and Environmental Sciences, University of Birmingham, B15 2TT, Birmingham, UK

▪ <sup>9</sup>Department of Meteorology, University of Reading, Reading, UK

▪ <sup>10</sup>Institut Pierre Simon Laplace, École Polytechnique, Palaiseau, France

<sup>11</sup>State Key Laboratory of Atmospheric Boundary Layer Physics and Atmospheric Chemistry, Institute for Atmospheric  
Physics, Chinese Academy of Sciences, 40 Huayanli, Chaoyang District, Beijing 100029, China

25 <sup>12</sup>Lancaster Environment Centre, Lancaster University, Lancaster, LA1 4YW, UK

<sup>13</sup>State Key Laboratory of Organic Geochemistry, Guangzhou Institute of Geochemistry, Chinese Academy of Sciences, 511  
Kehua Street, Wushan, Tianhe District, Guangzhou, GD 510640, China

<sup>14</sup>Institute of Surface-Earth System Science, Tianjin University, Tianjin 300072, China

<sup>a</sup>Now at: College of Environmental Sciences and Engineering, Peking University, Beijing, 100871, China

30 <sup>b</sup>Now at: Faculty of Science and Engineering, University of Chester, CH2 4NU, UK

<sup>c</sup>Now at: Aston Institute of Materials Research, School of Engineering and Applied Science, Aston University, Birmingham,  
B4 7ET, UK

<sup>d</sup>Now at: Turkish Accelerator & Radiation Laboratory, Ankara University Institute of Accelerator Technologies,  
Atmospheric and Environmental Chemistry Laboratory, Gölbaşı Campus, Ankara, Turkey

35 <sup>e</sup>Now at: Lancaster Environment Centre, Lancaster University, Lancaster, LA1 4YW, UK

<sup>f</sup>Now at: Department of Chemistry, York University, Toronto ON, M3J 1P3, Canada

*Correspondence to:* Lisa Whalley (l.k.whalley@leeds.ac.uk)



40

**Abstract.** Measurements of OH, HO<sub>2</sub>, RO<sub>2</sub>-complex (alkene and aromatic-related RO<sub>2</sub>) and total RO<sub>2</sub> radicals taken during the AIRPRO campaign in central Beijing in the summer of 2017, alongside observations of OH reactivity are presented. The concentrations of radicals were elevated with OH reaching up to  $2.8 \times 10^7$  molecule cm<sup>-3</sup>, HO<sub>2</sub> peaked at  $1 \times 10^9$  molecule cm<sup>-3</sup> and the total RO<sub>2</sub> concentration reached  $5.5 \times 10^9$  molecule cm<sup>-3</sup>. OH reactivity ( $k(\text{OH})$ ) peaked at  $89 \text{ s}^{-1}$  during the night, with a minimum during the afternoons of  $\sim 22 \text{ s}^{-1}$  on average. An experimental budget analysis, in which the rates of production and destruction of the radicals are compared, highlighted that although the sources and sinks of OH were balanced under high NO concentrations, the OH sinks exceeded the known sources (by  $15 \text{ ppbv hr}^{-1}$ ) under the very low NO conditions ( $< 0.5 \text{ ppbv}$ ) experienced in the afternoons, demonstrating a missing OH source consistent with previous studies under high volatile organic compound (VOC), low NO loadings. Under the highest NO mixing ratios ( $104 \text{ ppbv}$ ), the HO<sub>2</sub> production rate exceeded the rate of destruction by  $\sim 50 \text{ ppbv hr}^{-1}$ , whilst the rate of destruction of total-RO<sub>2</sub> exceeded the production by the same rate indicating that the net propagation rate of RO<sub>2</sub> to HO<sub>2</sub> may be substantially slower than assumed. If just 10% of the RO<sub>2</sub> radicals propagate to HO<sub>2</sub> upon reaction with NO, the HO<sub>2</sub> and RO<sub>2</sub> budgets could be closed at high NO, but at low NO this lower RO<sub>2</sub> to HO<sub>2</sub> propagation rate revealed a missing RO<sub>2</sub> sink that was similar in magnitude to the missing OH source. A detailed box model that incorporated the latest MCM chemical mechanism (MCM3.3.1) reproduced the observed OH concentrations well, but over-predicted the observed HO<sub>2</sub> under low concentrations of NO ( $< 1 \text{ ppbv}$ ) and under-predicted RO<sub>2</sub> (both the complex-RO<sub>2</sub> fraction and other RO<sub>2</sub> types which we classify as simple-RO<sub>2</sub>) most significantly at the highest NO concentrations. The model also under-predicted the observed  $k(\text{OH})$  consistently by  $\sim 10 \text{ s}^{-1}$  across all NO<sub>x</sub> levels highlighting that the good agreement for OH was fortuitous due to a cancellation of missing OH source and sink terms in its budget. Including heterogeneous loss of HO<sub>2</sub> to aerosol surfaces did reduce the modelled HO<sub>2</sub> concentrations in-line with the observations, but only at NO mixing ratios  $< 0.3 \text{ ppbv}$ . The inclusion of Cl atoms, formed from the photolysis of nitryl chloride, enhanced the modelled RO<sub>2</sub> concentration on several mornings when the Cl atom concentration was calculated to exceed  $1 \times 10^4$  atoms cm<sup>-3</sup> and could reconcile the modelled and measured RO<sub>2</sub> concentrations at these times. However, on other mornings, when the Cl atom concentration was lower, large under-predictions in total RO<sub>2</sub> remained. Furthermore, the inclusion of Cl atom chemistry did not enhance the modelled RO<sub>2</sub> beyond the first few hours after sunrise and so was unable to resolve the modelled under-prediction in RO<sub>2</sub> observed at other times of the day. Model scenarios, in which missing VOC reactivity was included as an additional reaction that converted OH to RO<sub>2</sub>, highlighted that the modelled OH, HO<sub>2</sub> and RO<sub>2</sub> concentrations were sensitive to the choice of RO<sub>2</sub> product. The level of modelled to measured agreement for HO<sub>2</sub> and RO<sub>2</sub> (both complex and simple) could be improved if the missing OH reactivity formed a larger RO<sub>2</sub> species that was able to undergo reaction with NO, followed by isomerisation reactions reforming other RO<sub>2</sub> species, before eventually generating HO<sub>2</sub>. In this work an  $\alpha$ -pinene-derived RO<sub>2</sub> species was used as an example. In this simulation, consistent with the experimental budget analysis, the model underestimated the observed OH indicating a missing OH source. The model uncertainty, with regards to the types of RO<sub>2</sub> species present and the radicals they form upon reaction with NO (HO<sub>2</sub> directly or another RO<sub>2</sub> species), leads to over an order of magnitude less O<sub>3</sub> production calculated from the predicted peroxy radicals than calculated from the observed

65  
70



75 peroxy radicals at the highest NO concentrations. This demonstrates the rate at which the larger RO<sub>2</sub> species propagate to HO<sub>2</sub> or to another RO<sub>2</sub> or indeed to OH needs to be understood to accurately simulate the rate of ozone production in environments such as Beijing where large multifunctional VOCs are likely present.

## 1 Introduction

Owing to strict emission controls being implemented across China, a reduction in the levels of PM<sub>10</sub>, PM<sub>2.5</sub> and SO<sub>2</sub> have been  
80 observed in the country since 2013 (Huang et al., 2018). Similar reductions in these primary pollutants are echoed in other countries across the globe. In the US this reduction in primary emissions is reflected in a ~0.4 ppbv yr<sup>-1</sup> reduction in peak O<sub>3</sub> (He et al., 2020). In China, however, despite reductions in primary emissions, the concentration of ground-level ozone has been gradually increasing between 2013 – 2017 (Huang et al., 2018). The highest peak ozone concentrations in China are observed in the Beijing area (Wang et al., 2017a) where the highest O<sub>3</sub> mixing ratio of 286 ppbv was recorded at a rural site  
85 50 km north of the centre (Wang et al., 2006). During the Beijing Olympic Games, despite emission controls, hourly ozone mixing ratios between 160 to 180 ppbv were frequently observed in central Beijing (Wang et al., 2010). Ozone is a secondary pollutant, primarily formed in the troposphere via OH-initiated VOC oxidation in the presence of NO<sub>x</sub>. O<sub>3</sub> concentrations in megacities worldwide frequently exceed regulatory limits during the summer months, with elevated ozone concentrations shown to have negative impacts on human and crop health. The radical species, OH, HO<sub>2</sub> and RO<sub>2</sub> play a central role in the  
90 catalytic photochemical cycle which removes primary emissions and leads to ozone formation. The OH radical initiates the oxidation of VOCs leading to the formation of peroxy radicals (HO<sub>2</sub> and RO<sub>2</sub>). Peroxy radicals oxidise NO to NO<sub>2</sub> which photolyses and generates ozone. Under high NO<sub>x</sub> conditions, OH preferentially reacts with NO<sub>2</sub>, and both peroxy radical production (via VOC oxidation) and, in turn, ozone production decreases. This non-linear relationship between ozone and NO<sub>x</sub> complicates efforts to reduce the ambient ozone levels as, in NO<sub>x</sub>-saturated environments, reductions in NO<sub>x</sub> can lead to  
95 increases in the rate of ozone production (e.g. (Bigi and Harrison, 2010)). Furthermore, a number of studies have highlighted that efforts to reduce PM have the potential to exacerbate O<sub>3</sub> due to concomitant increases in HO<sub>2</sub> caused by a reduction in the heterogeneous loss of HO<sub>2</sub> to aerosol surfaces (Li et al., 2019), although there is continued debate on the magnitude of this effect from field studies (Tan et al., 2020). As well as the central role OH plays in photochemical ozone formation, OH promotes the formation of secondary aerosols (sulphate, nitrate and secondary organic aerosols (SOA)) which have negative  
100 impacts on human health (Chen et al., 2013). Large, complex RO<sub>2</sub> radicals are precursors to highly oxidised molecules (HOMs) (Ehn et al., 2014) also which have been shown to condense and contribute to SOA (Mohr et al., 2019). In China, the fraction of PM attributed to secondary aerosols is significant (between 44 – 71%, (Huang et al., 2014)) and so understanding the oxidation chemistry which converts primary emissions to secondary aerosols is an ongoing challenge. There has been an increasing growth in photochemical oxidant studies conducted in China where radical observations have been performed over  
105 the past decade with the PKU and Juelich groups leading these efforts. The first radical observations took place in the summer



of 2006 with observations made in the Pearl River Delta region (Hofzumahaus et al., 2009; Lu et al., 2012) (PRIDE-PRD-2006) and also in suburban Beijing (Lu et al., 2013) (CareBeijing2006). These campaigns revealed a strong atmospheric oxidation capacity with elevated levels of OH and HO<sub>2</sub> in these regions, with OH concentrations up to 2.6 × 10<sup>7</sup> molecule cm<sup>-3</sup> and HO<sub>2</sub> concentrations up to 2.5 × 10<sup>9</sup> molecule cm<sup>-3</sup> reported (Lu et al., 2012). Even during the wintertime, under low  
110 levels of solar radiation, concentrations of OH can reach 3 × 10<sup>6</sup> molecule cm<sup>-3</sup> in Beijing (Slater et al., 2020) which is similar to the OH concentrations observed in other urban centres in European cities during the summer months (Whalley et al., 2018). Similar to findings from radical observations and subsequent modelling activities in forested regions (Whalley et al., 2011), which are characterised by high VOC emissions and relatively low NO<sub>x</sub> concentrations, the observations and modelling studies in China in summer (Hofzumahaus et al., 2009; Lu et al., 2012; Lu et al., 2013) revealed that the high OH concentrations could  
115 only be explained if an additional source of OH, from recycling peroxy radicals to OH, was added to the model. An updated isoprene scheme (Peeters et al., 2009; Peeters et al., 2014) which included isomerisation reactions of the isoprene-derived RO<sub>2</sub> radicals, was unable to reconcile the OH observations, however. In a subsequent field study conducted in the PRD region (Tan et al., 2019), RO<sub>2</sub> observations were made using the RO<sub>x</sub>LIF technique alongside OH, HO<sub>2</sub> and OH reactivity allowing an experimental budget analysis for OH, HO<sub>2</sub>, RO<sub>2</sub> and RO<sub>x</sub> (OH + HO<sub>2</sub> + RO<sub>2</sub>) to be performed. The analysis demonstrated a  
120 missing OH source of 4 – 6 ppbv hr<sup>-1</sup> and a missing RO<sub>2</sub> sink that was similar in magnitude and, hence, supports the hypothesis of a missing mechanism that converts RO<sub>2</sub> species to OH under low NO conditions. The authors calculated that the unknown RO<sub>2</sub> to OH conversion that does not involve reaction with NO (and, therefore, does not lead to the formation of ozone) reduced ozone production by 30 ppbv per day demonstrating that knowledge of the branching ratio between the competitive reactions that RO<sub>2</sub> radicals undergo (bimolecular reaction with NO or unimolecular isomerisation), as well as the overall VOC oxidation  
125 rate, is important when determining in situ ozone production.

In a recent campaign conducted at a rural site in the North China Plain (Tan et al., 2017), during periods for which NO mixing ratios were below 300 pptv, an additional OH recycling mechanism was again needed to reconcile the OH concentrations observed. The modelled RO<sub>2</sub> concentrations were in good agreement with those observed under low NO concentrations typically experienced during the afternoon, however, the model under-predicted the RO<sub>2</sub> concentrations by a factor of 3 - 5 at  
130 the higher NO mixing ratios (>1 ppbv) that were observed during the mornings. Additional sources of RO<sub>2</sub> from the photolysis of ClNO<sub>2</sub> and subsequent reactions of Cl atoms with VOCs, as well as RO<sub>2</sub> from the missing reactivity determined, could explain ~ 10 – 20% of the model under-prediction, but could not fully resolve the missing RO<sub>2</sub> source of 2ppbv hr<sup>-1</sup> under the high NO conditions. As a result, the model was found to under-predict the net in situ chemical ozone production by 20 ppbv per day. In London, during the ClearLo campaign (Whalley et al., 2018), under higher NO mixing ratios (> 3ppbv) a box  
135 model constrained to the MCM3.2 was found to increasingly under-predict the RO<sub>2</sub> concentrations observed with NO<sub>x</sub> and, as a consequence the rate of ozone production calculated from the modelled peroxy radical concentrations was up to an order of magnitude lower than the ozone production rate calculated from the observed peroxy radicals. The model was able to reproduce



the observed levels of HO<sub>2</sub> under the high NO concentrations, but over-predicted HO<sub>2</sub> concentrations when NO mixing ratios were below 1 ppbv and modest under-predictions of OH were observed under low NO conditions which demonstrated  
140 uncertainties in radical cycling at low NO. Conversely, in other urban studies, models were found to increasingly under-predict HO<sub>2</sub> as NO<sub>x</sub> levels increased beyond ~ 1 ppbv (Martinez et al., 2003; Ren et al., 2013; Brune et al., 2016) although in some of these earlier studies, the HO<sub>2</sub> observations may have been influenced by an RO<sub>2</sub> interference (Whalley et al., 2013). Understanding the cause of the model failure under different NO regimes in urban centres is critical to be able to accurately predict ozone production and to determine ozone abatement strategies that can be implemented to successfully reduce ozone  
145 levels. Measurements of OH, HO<sub>2</sub> and RO<sub>2</sub> as well as OH reactivity are necessary to fully explore a model's skill to capture the entire atmospheric oxidation cycle and to begin to identify mechanisms that can reconcile the concentration of all radical species.

The integrated Study of AIR Pollution PROcesses in Beijing (AIRPRO) project involved two intensive measurement periods that took place in central Beijing during the winter of 2016 and during the following summer of 2017 and was part of the larger  
150 Air Pollution and Human Health (APHH) program. APHH had the overall aim of better understanding the sources, atmospheric transformations and health impacts of air pollutants in Beijing to improve air quality forecasting capabilities (Shi et al., 2019). In this paper the observations of OH, HO<sub>2</sub>, RO<sub>2</sub> and OH reactivity from the summer period are compared to a detailed zero dimensional box model run with the latest Master Chemical Mechanism (MCM3.3.1) and an experimental budget analysis is performed on all radical species. The overall objective of this research was to test the model's ability to reproduce the radical  
155 concentrations and, through the budget analysis investigate the balance between radical production and destruction rates. Following on from the results of earlier radical observation and modelling studies conducted in urban regions, this research will investigate if there are missing radical sources and sinks under different NO regimes and investigate new chemistry that may improve model predictions. We will assess how uncertainties in the model mechanism influence the rate of in situ ozone production in an environment with large and complex VOC emissions and under highly variable NO<sub>x</sub> concentrations.

## 160 **2 Experimental**

### **2.1 Site description**

The observations took place in central Beijing at the Institute of Atmospheric Physics (IAP), which is part of the Chinese Academy of Sciences. The site was located between the third and fourth north ring roads in Beijing and was within 150 m of several busy roads. All instrumentation was located in close proximity within 9 shipping containers that were placed on a



165 grassed area surrounding a large (325 m) meteorological tower. Further details of the measurement site and an overview of all  
the instrumentation that was run during the campaign can be found in Shi et al., (2019).

## 2.2 FAGE instrumentation

The University of Leeds fluorescence assay by gas expansion (FAGE) instrument was deployed at the IAP site and made  
measurements of OH, HO<sub>2</sub>, RO<sub>2</sub> radicals and OH reactivity (k(OH)). The instrumental set-up was analogous to that used during  
170 the ClearfLo project (see Whalley et al., (2016) for the k(OH) instrument description and Whalley et al., (2018) for the OH,  
HO<sub>2</sub>, and RO<sub>2</sub> instrument details) and also the winter AIRPRO project (Slater et al., 2020) and so is only briefly overviewed  
here. Two detection cells, the HO<sub>x</sub> cell and the RO<sub>x</sub>LIF cell, were located on the roof of the Leeds FAGE shipping container  
at a sampling height of 3.5 m. The k(OH) instrument, which was housed inside the container, alongside all other FAGE  
instrument components (including the laser system), drew air from close by the radical detection cells via an 1/2" Teflon line.  
175 The HO<sub>x</sub> cell made sequential measurements of OH and then the sum of OH + HO<sub>2</sub>, by the addition of NO (Messer, 99.95%)  
which titrated HO<sub>2</sub> to OH for detection by laser induced fluorescence (LIF). In the RO<sub>x</sub>LIF reactor, in HO<sub>x</sub>-mode, a flow of  
CO (10% in N<sub>2</sub>) was added just beneath the sampling inlet and this rapidly converted any ambient OH sampled to HO<sub>2</sub>. Within  
the RO<sub>x</sub>LIF FAGE cell, a continuous flow of NO (99.95%) titrated ambient HO<sub>2</sub>, the converted OH and also a large % of RO<sub>2</sub>-  
complex radicals (see below) to OH for detection. In RO<sub>x</sub>-mode, a total-RO<sub>2</sub> + HO<sub>2</sub> + OH measurement was made by addition  
180 of a dilute flow of NO (500 ppmv in N<sub>2</sub>) alongside the CO which promoted the conversion of all HO<sub>2</sub> and RO<sub>2</sub> radicals to OH;  
the OH formed was rapidly re-converted to HO<sub>2</sub> by reaction with CO. Within the RO<sub>x</sub>LIF FAGE cell, the HO<sub>2</sub> was titrated  
back to OH, by reaction with NO, for detection. Using the methodology outlined in Whalley et al., (2013) the sensitivity of  
both the HO<sub>x</sub> and RO<sub>x</sub>LIF FAGE cells towards HO<sub>2</sub> and RO<sub>2</sub>-complex species was assessed before the instrument was  
deployed to Beijing by sampling isoprene-derived RO<sub>2</sub>; the sensitivity of the HO<sub>x</sub> cell towards other RO<sub>2</sub> types such as those  
185 derived from ethene, methanol and propane has been previously conducted (Whalley et al., 2013) and compared well with  
model-predicted sensitivities. The sensitivity of the RO<sub>x</sub>LIF instrument has also been assessed previously towards a range of  
RO<sub>2</sub> types deriving from methane, isoprene, ethene, toluene, butane and cyclohexane and, again, compared well with model-  
predicted sensitivities (Whalley et al., 2018). RO<sub>2</sub>-complex refers to any RO<sub>2</sub> species (primarily those derived from alkene and  
aromatic hydrocarbons) that have the potential to decompose into OH in the presence of NO on the time-scale of the FAGE  
190 residence time and, therefore, have the potential to act as an HO<sub>2</sub> interference. The NO flow in the HO<sub>x</sub> cell was kept low to  
minimise the conversion efficiency of RO<sub>2</sub>-complex to OH and the conversion efficiency was found to be <5% when isoprene-  
derived RO<sub>2</sub> radicals were sampled. In the RO<sub>x</sub>LIF FAGE cell, a higher NO flow was employed to promote the conversion of  
RO<sub>2</sub>-complex to OH, enabling 89% of isoprene-derived RO<sub>2</sub> radicals to be detected. From the relative sensitivities of the two



195 cells to OH, HO<sub>2</sub> and RO<sub>2</sub>-complex, and by subtraction of RO<sub>2</sub>-complex from total RO<sub>2</sub>, the concentration of RO<sub>2</sub> species that do not act as an HO<sub>2</sub> interference (RO<sub>2</sub>-simple) has been derived.

For the entirety of the campaign, the HO<sub>x</sub> cell was equipped with an inlet-pre-injector (IPI) (Woodward-Massey et al., 2020) which, by injection of propane into the ambient air-stream directly above the HO<sub>x</sub> inlet, removes ambient OH and enables a background measurement from laser scatter, solar scatter and detector dark counts (and potentially any cell-generated OH) to be determined whilst the laser is tuned to the OH transition. The subtraction of this background signal from the ambient OH  
200 signal provides the OH<sub>CHEM</sub> measurement which can be compared to the traditional OH<sub>WAVE</sub> measurement in which the background signal (from laser scatter, solar scatter and detector dark counts only) is determined by tuning the laser wavelength away from the OH transition. Differences between OH<sub>CHEM</sub> and OH<sub>WAVE</sub> can highlight the presence of an OH interference. During the summer AIRPRO campaign, once the known OH interference deriving from laser-photolysis of ambient ozone and the subsequent reaction of photogenerated O(<sup>1</sup>D) atoms with ambient H<sub>2</sub>O (v) was accounted for (Woodward-Massey et al.,  
205 2020) the agreement between OH<sub>CHEM</sub> and OH<sub>WAVE</sub> was generally very good (see figure 14 in Woodward-Massey et al., (2020)). However, on five afternoons when ozone was extremely elevated (>100 ppbv) and OH concentrations were high (>1x10<sup>7</sup> cm<sup>-3</sup>), OH<sub>WAVE</sub> was greater than OH<sub>CHEM</sub> (by up to 18 %) highlighting a small unknown interference under these very perturbed conditions. In all the model-measurement comparisons presented in the section 3, the interference-free OH<sub>CHEM</sub> measurement is used.

210 Both detection cells were calibrated every 3 days during the campaign by photolysis of a known concentration of H<sub>2</sub>O (v) at 185 nm with a Hg lamp in synthetic air (Messer, Air Grade Zero 2) within a turbulent flow tube which generates an equal concentration of OH and HO<sub>2</sub> (Whalley et al. 2018). The product of the photon flux at 185 nm (determined by N<sub>2</sub>O actinometry (Commane et al., 2010) before and after the instrument was deployed to Beijing), [H<sub>2</sub>O] and irradiance time, was used to calculate [OH] and [HO<sub>2</sub>]. For calibration of RO<sub>2</sub> concentrations, methane (Messer, Grade 5, 99.99%) was added to the  
215 humidified air flow in sufficient quantity to completely convert OH to CH<sub>3</sub>O<sub>2</sub>. The median limit of detection (LOD) during the campaign was 6.1 × 10<sup>5</sup> molecule cm<sup>-3</sup> for OH, 2.8 × 10<sup>6</sup> molecule cm<sup>-3</sup> for HO<sub>2</sub> and 7.2 × 10<sup>6</sup> molecule cm<sup>-3</sup> for CH<sub>3</sub>O<sub>2</sub> at a typical laser power of 11 mW for a 5 minute data acquisition cycle (SNR=2). The field measurements of all species were recorded with 1 s time-resolution, and the precision of the measurements was calculated using the standard errors in both the  
220 online and offline points. The accuracy of the measurements was ~ 26 % (2σ), and is derived from uncertainties in the calibration, which derives largely from that of the chemical actinometer (Commane et al., 2010).

### 2.3 Experimental budget analysis

An experimental budget analysis has been conducted for OH, HO<sub>2</sub>, RO<sub>2</sub>, and total RO<sub>x</sub> following the approach outlined in Tan et al., (2019) and which relies only on field-measured quantities (concentrations and photolysis rates) and published chemical



kinetic data, and not any model calculated concentrations. The rates of production and destruction of each radical species is  
 225 calculated using equations 1 – 8 below.

$$P_{\text{OH}} = j_{\text{HONO}}[\text{HONO}] + (2f \times j_{\text{O}^1\text{D}}[\text{O}_3]) + \sum_i \{ \varphi_{\text{OH}}^i k_{i1}^i [\text{alkene}]_i [\text{O}_3] \} + (k_2[\text{NO}] + k_3[\text{O}_3])[\text{HO}_2] \quad (1)$$

$$D_{\text{OH}} = [\text{OH}]k_{\text{OH}} \quad (2)$$

230  $P_{\text{HO}_2} = 2j_{\text{HCHO}_r}[\text{HCHO}] + \sum_i \{ \varphi_{\text{HO}_2}^i k_{i1}^i [\text{alkene}]_i [\text{O}_3] \} + (k_4[\text{HCHO}] + k_5[\text{CO}])[\text{OH}] + \alpha k_6[\text{NO}][\text{RO}_2] \quad (3)$

$$D_{\text{HO}_2} = (k_7[\text{NO}] + k_8[\text{O}_3] + k_9[\text{RO}_2] + k_{\text{het}} + 2k_{10}[\text{HO}_2])[\text{HO}_2] \quad (4)$$

$$P_{\text{RO}_2} = \sum_i \{ \varphi_{\text{RO}_2}^i k_{i1}^i [\text{alkene}]_i [\text{O}_3] \} + k_{\text{OH}[\text{VOC}]}[\text{OH}] \quad (5)$$

$$D_{\text{RO}_2} = \{ (\alpha + \beta)k_6[\text{NO}] + (2k_{11}[\text{RO}_2] + k_9[\text{HO}_2])[\text{RO}_2] \} \quad (6)$$

235

$$P_{\text{RO}_x} = j_{\text{HONO}}[\text{HONO}] + 2f \times j_{\text{O}^1\text{D}}[\text{O}_3] + 2j_{\text{HCHO}_r}[\text{HCHO}] + \sum_i \{ (\varphi_{\text{OH}}^i + \varphi_{\text{HO}_2}^i + \varphi_{\text{RO}_2}^i) k_{i1}^i [\text{alkene}]_i [\text{O}_3] \} \quad (7)$$

$$D_{\text{RO}_x} = (k_{12}[\text{NO}_2] + k_{13}[\text{NO}])[\text{OH}] + \beta k_6[\text{NO}][\text{RO}_2] + 2(k_{11}[\text{RO}_2]^2 + k_9[\text{RO}_2][\text{HO}_2] + k_{10}[\text{HO}_2]^2) \quad (8)$$

where  $j_{\text{HONO}}$  and  $j_{\text{O}^1\text{D}}$  are the measured photolysis rates of HONO and O<sub>3</sub> (forming O<sup>1</sup>D) respectively,  $f$  is the fraction of O<sup>1</sup>D  
 240 radicals that react with H<sub>2</sub>O rather than are collisionally quenched to O(<sup>3</sup>P) ( $f = 0.1$  on average) and  $\varphi_{\text{OH}}^i$ ,  $\varphi_{\text{HO}_2}^i$ ,  $\varphi_{\text{RO}_2}^i$  and  
 $k_{i1}^i$  are the yield of OH, HO<sub>2</sub> and RO<sub>2</sub> from, and rate coefficients for, individual ozone-alkene reactions taken from the  
 MCM3.3.1 respectively.  $j_{\text{HCHO}_r}$  is the measured HCHO photolysis rate that yields HO<sub>2</sub> radicals,  $k_{\text{het}}$  is the first order loss of  
 HO<sub>2</sub> to the measured aerosol surface area, calculated using Eq.9:

$$k_{\text{het}} = \frac{\omega A \gamma}{4} \quad (9)$$

245 where  $\omega$  is the mean molecular speed of HO<sub>2</sub> (equal to 43725 cm s<sup>-1</sup> at 298 K),  $\gamma$  is the aerosol uptake coefficient (0.2 is used  
 here as recommended by Jacob (2000)) and  $A$  is the measured aerosol surface area in cm<sup>2</sup>cm<sup>-3</sup>.  $\alpha$  is the fraction of RO<sub>2</sub> radicals  
 that upon reaction with NO propagate to HO<sub>2</sub> rather than reform another RO<sub>2</sub> radical; initially  $\alpha = 1$  has been assumed.  $\beta$  is  
 the fraction of RO<sub>2</sub> radicals that upon reaction with NO form alkyl nitrates and is set to 0.05 as used by Tan et al., (2019) to  
 250 represent an average alkyl nitrate yield for the various types of RO<sub>2</sub> species likely present. All rate coefficients ( $k_1 - k_{13}$ ) used  
 are listed in Table 1 and the concentration of species used in the budget analysis are the concentrations that were observed  
 during the campaign.



## 2.4 MCM3.3.1 box model description

A zero-dimensional (box) model incorporating the Master Chemical Mechanism (MCM3.3.1) (Jenkin et al., 2015) (http://mcm.leeds.ac.uk/MCM/home) was used to predict the radical concentrations and OH reactivity for comparison with the observations. The model was constrained by measurements of NO, NO<sub>2</sub>, NO<sub>3</sub>, O<sub>3</sub>, CO, HCHO, HNO<sub>3</sub>, HONO, water vapour, temperature, pressure and individual VOC species measured by DC-GC-FID (dual-channel gas chromatography with flame ionisation) and PTR-ToF-MS (proton transfer reactor-time of flight-mass spectrometry). Table 2 lists the different VOC species measured. HCHO was measured using a recently developed LIF instrument with 1 sec time resolution and LOD of 80 pptv (Cryer, 2016). HONO was measured by a long-path absorption photometer (LOPAP) and broadband cavity-enhanced absorption spectrophotometry (BBCEAS) and the HONO concentration as recommended in Crilley et al., (2019) are used here. Further details on all instrumentation deployed during the campaign is overviewed in Shi et al. (2019).

The model was constrained with the measured photolysis frequencies  $j(\text{O}^1\text{D})$ ,  $j(\text{NO}_2)$  and  $j(\text{HONO})$ , which were calculated from the measured wavelength-resolved actinic flux and published absorption cross sections and photodissociation quantum yields. For other species which photolyse at near-UV wavelengths (<360 nm), such as HCHO and CH<sub>3</sub>CHO, the photolysis rates were calculated by scaling to the ratio of clear-sky  $j(\text{O}^1\text{D})$  to observed  $j(\text{O}^1\text{D})$  to account for clouds. For species which photolyse further into the visible the ratio of clear-sky  $j(\text{NO}_2)$  to observed  $j(\text{NO}_2)$  was used. The variation of the clear-sky photolysis rates ( $j$ ) with solar zenith angle ( $\chi$ ) was calculated within the model using the following expression:

$$j = l \cos(\chi) m \times e^{-n \sec(\chi)} \quad (10)$$

with the parameters  $l$ ,  $m$  and  $n$  optimised for each photolysis frequency (see Table 2 in Saunders et al., (2003)). The model inputs were updated every 15 minutes, the species that were measured more frequently were averaged to 15 minutes whilst the measurements with lower time resolution were interpolated. To estimate how long model generated intermediate species survive before being physically removed by processes such as deposition or ventilation, the model was left unconstrained to glyoxal and the rate of physical loss was varied. The model was able to reproduce the observed glyoxal concentrations if a deposition velocity of 0.5 cm s<sup>-1</sup> was used, combined with a ventilation term that increased with the measured boundary layer depth (Kotthaus and Grimmond, 2018). As the boundary layer gradually increased in the morning, the lifetime of glyoxal with respect to ventilation was ~ 1 hour, whilst at night the lifetime gradually increased to ~ 5 hours; this variable lifetime was applied to all model-generated species. As a further check on the physical loss rate imposed, the model was run unconstrained to HCHO using the same deposition rates and was found to reproduce the observed HCHO concentrations that were observed during the daytime, but under-predicted the concentrations at night, potentially indicating that primary emissions of HCHO as



well as secondary production contributed to the observed concentrations. In all the model scenarios presented in section 3, the observed HCHO concentration is used. The model was run for the entirety of the campaign in overlapping 7 day segments. To allow all the unmeasured, model generated intermediate species time to reach steady state concentrations, the model was initialised with inputs from the first measurement day and spun-up for 2 days before comparison to measurements of OH, HO<sub>2</sub>, RO<sub>2</sub> and k(OH) were made. For comparison of the modelled RO<sub>2</sub> to the observed RO<sub>2</sub>-total, RO<sub>2</sub>-complex and RO<sub>2</sub>-simple, the RO<sub>x</sub>LIF instrument sensitivity towards each RO<sub>2</sub> species in the model was determined by running a model first under the RO<sub>x</sub>LIF reactor and then the RO<sub>x</sub>LIF FAGE cell conditions (NO concentrations and residence times) to determine the conversion efficiency of each modelled RO<sub>2</sub> species to HO<sub>2</sub>.

### 2.4.1 Model descriptions

A series of model runs have been performed and are summarised in Table 3:

## 3 Results and Discussion

### 3.1 Overview of the chemistry and meteorology during the campaign

As part of the AIRPRO project, gas-phase, aerosol, and meteorological observations were made at the IAP site from the 21<sup>st</sup> May to 26<sup>th</sup> June in 2017. Typically clear skies and elevated temperatures prevailed, with rain on just a few days. Temperatures frequently exceeded 35 °C whilst j(O<sup>1</sup>D) peaked at just over  $3 \times 10^{-5} \text{ s}^{-1}$  at noon (Figure 1). The dominant wind direction reaching the site during the summer was from the southwest and the measured hourly mean wind speed was  $3.6 \text{ ms}^{-1}$  (Shi et al., 2019). Despite the close proximity of the measurement site to the heavily trafficked Jingzang highway in Beijing, mixing ratios of NO, which were elevated during the morning hours, often dropped below 500 pptv during the afternoon. The daytime emissions of NO<sub>x</sub> that were recorded during the project displayed a rapid increase at 05:00 and then remained reasonably constant throughout the day, with a mean flux value of  $4.6 \text{ mg m}^{-2} \text{ hr}^{-1}$ , before dropping again at 17:00 (Squires et al., 2020). The rapid decrease in NO into the afternoon, therefore, was not driven by a change in emissions, but rather instead by the increasing boundary layer depth and also by the chemistry, as elevated levels of ozone observed in the afternoon effectively titrated NO to NO<sub>2</sub> (Newland et al., 2020). Isoprene mixing ratios also peaked in the afternoon, often reaching a few ppbv, indicative of a biogenic source. The variation in NO<sub>x</sub> and VOC concentrations experienced at the site provides an opportunity to assess the skill of the MCM to capture the complex chemistry occurring over an extremely wide range of chemical regimes that encompasses both typical urban conditions (high NO<sub>x</sub>) as well as chemical conditions more akin to forested environments (low NO, high BVOC). From the 9<sup>th</sup> – 12<sup>th</sup> June, NO levels were elevated throughout the day suggesting a local source, whilst from the 17<sup>th</sup> June to the end of the measurement period, NO concentrations dropped and, so as well as the strong diurnal trend observed in the NO concentration, these periods provide further opportunity to test the model's ability to predict radical



310 concentrations as a function of NO by removing concomitant variables such as changing boundary layer depth and sunrise  
which occurred in unison with the morning increase in NO concentration.

### 3.2 Radical concentrations and OH reactivity

The concentrations of RO<sub>x</sub> (OH + HO<sub>2</sub> + RO<sub>2</sub>) radicals were high during the campaign (Figure 2), with OH concentrations  
315 frequently exceeded 1 x 10<sup>7</sup> molecule cm<sup>-3</sup> and reaching up to 2.8 x 10<sup>7</sup> molecule cm<sup>-3</sup> on the 30<sup>th</sup> May. These OH levels are  
amongst the highest measured in an urban environment (Lu et al., 2019), and are comparable to the OH concentrations observed  
in the Pearl River Delta downwind of the Southern Chinese megacity of Guangzhou, where OH concentrations reached 2.6 x  
10<sup>7</sup> molecule cm<sup>-3</sup> (Lu et al., 2012). HO<sub>2</sub> concentrations peaked at 1 x 10<sup>9</sup> molecule cm<sup>-3</sup> on the 9<sup>th</sup> June, whilst the highest  
320 concentrations of total RO<sub>2</sub> were observed during the latter half of the campaign, peaking at 5.5 x 10<sup>9</sup> molecule cm<sup>-3</sup> on the  
afternoon of the 15<sup>th</sup> June. RO<sub>2</sub> measurements, alongside OH and HO<sub>2</sub>, were, until recently, relatively rare. OH and RO<sub>x</sub> were  
measured during the MEGAPOLI project in Paris (Michoud et al., 2012) where the average daytime maximum concentrations  
of RO<sub>x</sub> were 1.2 x 10<sup>8</sup> molecule cm<sup>-3</sup> which is over an order of magnitude lower than the levels observed in Beijing. Since the  
development of the RO<sub>x</sub>LIF technique, (Fuchs et al., 2008), RO<sub>2</sub> observations are now reported by the Leeds, Juelich and PKU  
FAGE groups. RO<sub>2</sub> concentrations observed in London in the summer reached up to 5.5 x 10<sup>8</sup> molecule cm<sup>-3</sup> in air masses that  
325 had previously passed over central London (Whalley et al., 2018). In Wangdu, a town situated on the North China Plain, 170  
km northeast of Beijing, summertime RO<sub>2</sub> concentrations reached up to 1.5 x 10<sup>9</sup> molecule cm<sup>-3</sup> (Tan et al., 2017) which,  
although lower than observed in central Beijing, are much higher than observed in the summertime in European cities  
suggesting that there may be significant differences in the urban photochemistry occurring in China and Europe.

330 As well as the elevated daytime radical concentrations, concentrations of OH, HO<sub>2</sub> and RO<sub>2</sub> remained elevated above the  
instrumental LOD on most nights. The high night-time OH concentrations (ranging from the LOD up to 2 x 10<sup>6</sup> molecule  
cm<sup>-3</sup>) are comparable to the levels of OH observed at night in Yufa (a suburb of Beijing) and downwind of Guangzhou where  
night-time OH concentrations ranged from 0.5 – 3 x 10<sup>6</sup> molecule cm<sup>-3</sup> (Lu et al., 2014). The observations of OH from the  
earlier China campaigns could be reconciled by a model if an additional RO<sub>x</sub> production process was included which recycled  
335 RO<sub>2</sub> to OH via HO<sub>2</sub>. A weak positive correlation is observed between night-time OH and RO<sub>2</sub> at night during AIRPRO and  
the secondary peak in RO<sub>2</sub> occurred when NO<sub>3</sub> was observed to increase rapidly at ~19:30 suggesting that nitrate chemistry  
was one source of radicals in the evening. Alkyl nitrates, formed from aldehydes + NO<sub>3</sub> were also enhanced at these times at  
this site (Reeves et al., 2019).

340 The OH reactivity, typical of urban environments displayed an inverse relationship with boundary layer height and was highest  
during the nights when emissions were compressed into a lower boundary layer depth of ~150 m. An average maximum of  
k(OH) ~37 s<sup>-1</sup> was observed at 06:00 with OH reactivity reaching 89 s<sup>-1</sup> on the 15<sup>th</sup> June at 03:00. During the daytime the OH



345 reactivity dropped to a minimum of  $\sim 22 \text{ s}^{-1}$  on average at  $\sim 15:00$  when the boundary layer had increased to  $\sim 1500 \text{ m}$ . The magnitude of OH reactivity observed during AIRPRO is comparable to the OH reactivity observed at other urban sites in China in the summer (Lou et al., 2010; Fuchs et al., 2017) and also in Tokyo during the summer (Sadanaga et al., 2004; Chatani et al., 2009). In London, OH reactivity was approximately  $\sim 7 - 10 \text{ s}^{-1}$  lower than in central Beijing with  $\sim 15 \text{ s}^{-1}$  observed during the day on average and an average maximum of  $\sim 27 \text{ s}^{-1}$  at 06:00 (Whalley et al., 2016). Lower OH reactivities are also reported from US urban sites in New York and Texas (Ren et al., 2003; Mao et al., 2010).

### 350 3.3 Experimental Radical Budget Analysis

Owing to the relatively short-lifetime of radicals, it can be assumed that their production rates and destruction rates are balanced. A comparison of the rates of production and destruction for each radical species can be used to help identify if all radical sources and sinks are accounted for and if the rates of propagation between radical species is fully understood. In London, the ratio of the OH production rate (Eq. 1) to OH destruction rate (Eq.2) was generally close to 1 throughout the campaign demonstrating consistency between the OH, HO<sub>2</sub>, k(OH), HONO and NO observations (Whalley et al., 2018). However, under low NO conditions ( $< 0.5 \text{ ppbv}$ ) the rate of OH destruction exceeded the calculated production rate indicating that Eq.1 was missing a source term under these regimes (Whalley et al., 2018). A steady-state analysis of HO<sub>2</sub> conducted for the London project which balanced the HO<sub>2</sub> production terms (Eq.3) with the first and second order loss terms (Eq.4) highlighted that closure between the production and destruction terms could only be reconciled if the rate of propagation of the observed RO<sub>2</sub> radicals to HO<sub>2</sub> was decreased substantially to just 15%, demonstrating that the mechanism by which RO<sub>2</sub> radicals propagate to other radical species may not be well understood (Whalley et al., 2018). As set out by Tan et al., (2019), analogous budget analyses can be performed for RO<sub>2</sub> species (Eq.5 – Eq.6) and for the entire RO<sub>x</sub> budget (Eq.7 – Eq.8). Tan et al., (2019) found that the production and destruction terms for RO<sub>2</sub> were balanced in the mornings in the PRD, when the measured OH reactivity was used to calculate the rate of RO<sub>2</sub> production from VOC+OH reactions, but during the afternoon a missing RO<sub>2</sub> sink ( $2 - 5 \text{ ppbv hr}^{-1}$ ) was evident. In the PRD study (Tan et al., 2019), the OH destruction rate exceeded the production rate by  $4 - 6 \text{ ppbv hr}^{-1}$  in the afternoon, but, in contrast to London (Whalley et al., 2018), the HO<sub>2</sub> budget was closed throughout the whole day. The total rate of RO<sub>x</sub> production and destruction were in good agreement in the PRD (Tan et al., 2019).

370 A comparison of the campaign median production and destruction rates for RO<sub>x</sub>, OH, HO<sub>2</sub> and RO<sub>2</sub> during AIRPRO are presented in figure 3. The total rate of RO<sub>x</sub> production and destruction are in good agreement throughout the day from  $\sim 10 \text{ am}$ . A night-time source of radicals of just under  $1 \text{ ppbv hr}^{-1}$  is missing from the budget analysis likely reflecting missing production from NO<sub>3</sub> + VOC reactions (night-time radical production is considered further in section 3.5). From 6 am to 10 am, the RO<sub>x</sub> destruction exceeds the production by up to  $4 \text{ ppbv hr}^{-1}$  indicating a substantial,  $\sim 50\%$ , missing primary RO<sub>x</sub> source at this time. Previous work has suggested that Cl-initiated VOC oxidation may be an important source of RO<sub>2</sub> radicals in urban



regions (Riedel et al., 2014; Bannan et al., 2015; Tan et al., 2017) but has not been included in the RO<sub>x</sub> or RO<sub>2</sub> production rate calculations here. Nitryl chloride was measured for part of the AIRPRO campaign and the impact of this on the modelled RO<sub>2</sub> concentration is investigated in section 3.4. The total RO<sub>x</sub> production and destruction rate is of the order of 6 ppbv hr<sup>-1</sup> at noon which is slightly faster than in the PRD, where a median peak total radical production rate of ~4 ppbv hr<sup>-1</sup> was calculated. The median OH destruction rate is ~ 30 ppbv hr<sup>-1</sup> at noon and is roughly twice as fast the production rate at this time highlighting a large missing source of OH radicals in the budget (~ 15 ppbv hr<sup>-1</sup>). Although a missing OH source was also reported in the PRD (Tan et al., 2019), the missing production rate is ~ 3 times faster during AIRPRO. The known OH production rate during AIRPRO is dominated by the reaction of HO<sub>2</sub> with NO (contributing ~60 % during the day to P(OH) in Eq.1). The median peak HO<sub>2</sub> production of ~60 ppbv hr<sup>-1</sup> is observed in the morning hours and greatly exceeded the known rate of HO<sub>2</sub> destruction by ~ 50 ppbv hr<sup>-1</sup>. HO<sub>2</sub> production is driven by the reaction of RO<sub>2</sub> with NO which accounts for 88% of the total. The reaction of OH with CO and HCHO accounts for a further 9%. The total HO<sub>2</sub> production rate is approximately 4 times faster than that calculated for the PRD (Tan et al., 2019). The total rate of RO<sub>2</sub> destruction mirrors the HO<sub>2</sub> production in that it is dominated by the reaction of RO<sub>2</sub> radicals with NO. From sunrise – 14:00 the rate of RO<sub>2</sub> destruction is faster than RO<sub>2</sub> production by up to 50 ppbv hr<sup>-1</sup>. After 14:00 the rate of RO<sub>2</sub> production and destruction are in good agreement. This trend contrasts with the budget analysis presented from PRD (Tan et al., 2019), which highlighted a possible missing RO<sub>2</sub> sink during the afternoon hours and budget closure in the morning hours.

Binning the ratio of P(OH) to D(OH), P(HO<sub>2</sub>) to D(HO<sub>2</sub>) and P(RO<sub>2</sub>) to D(RO<sub>2</sub>) against NO mixing ratio (figure 4) reveals that the RO<sub>2</sub> budget is in good agreement at the lowest NO mixing ratios but as NO mixing ratios increase the destruction of RO<sub>2</sub> becomes faster than production of RO<sub>2</sub> by up to a factor of 10 at the highest NO bin. The trends in the RO<sub>2</sub> and HO<sub>2</sub> ratios are similar in the morning hours, albeit in opposite directions, and suggests that rather than there being a missing primary source of RO<sub>2</sub> and missing sink for HO<sub>2</sub> that happen to balance, instead, as found in London (Whalley et al., 2018), the net propagation rate of RO<sub>2</sub> to HO<sub>2</sub> may be substantially slower than the rate that has currently been used in this analysis. In London (Whalley et al., 2018), the modelled rate of production analysis revealed that only ~50% of the total RO<sub>2</sub> species propagated to HO<sub>2</sub> following reaction with NO, as a significant fraction of the alkoxy radicals formed (such as those generated during the oxidation of monoterpenes and long-chain alkanes) preferentially isomerised and reformed a more oxidised RO<sub>2</sub> species in the presence of O<sub>2</sub> instead. In the London model radical flux analysis using the MCM3.2, (Whalley et al., 2018), the propagation of alkyl- and acyl-RO<sub>2</sub> species were combined and so the interconversion of acyl-RO<sub>2</sub> radicals (from the OH-initiated oxidation of aldehydic VOCs, photolysis of ketones and decomposition of PAN species) to alkyl-RO<sub>2</sub> radicals following reaction with NO was not explicitly shown, but this interconversion of one RO<sub>2</sub> species to another would serve to reduce the fraction of RO<sub>2</sub> radicals that propagate to HO<sub>2</sub> further. Thus far for AIRPRO, the experimental budget analysis has assumed that 95% of the measured RO<sub>2</sub> species, upon reaction with NO, produce HO<sub>2</sub>. If, however, a large fraction of the total RO<sub>2</sub> measured derive from long-chain alkanes, monoterpenes or acyl-RO<sub>2</sub> species, the budget analysis will over-estimate HO<sub>2</sub>



410 production and also the net RO<sub>2</sub> destruction, as the reaction of these peroxy radicals with NO effectively converts one RO<sub>2</sub>  
species to another RO<sub>2</sub> species, and so the reaction with NO will be neutral in terms of RO<sub>2</sub> production and destruction. Taking  
 $\alpha = 0.1$  leads to a good agreement between the production and destruction rates of HO<sub>2</sub> over the whole day and the observed  
range of NO. The production and destruction rates of RO<sub>2</sub> agree under high NO conditions, but at NO mixing ratios <5 ppbv  
the production of RO<sub>2</sub> exceeds the destruction, highlighting (if this  $\alpha$  value is correct) that there is a missing RO<sub>2</sub> sink at the  
415 lower NO concentrations. Tan et al., (2019) also report a missing RO<sub>2</sub> sink under low NO conditions during PRD and suggested  
that autoxidation of RO<sub>2</sub> species could account for this missing sink and may also possibly act as the missing source of OH  
identified under the low NO conditions. An additional first order reaction that converts RO<sub>2</sub> to OH at a rate of 0.1 s<sup>-1</sup> brings  
the P:D(OH) and P:D(RO<sub>2</sub>) ratios close to 1 at all NO mixing ratios >0.3 ppbv, but at low NO mixing ratios (0.1 – 0.3 ppbv  
range) an even slower rate of conversion is required, highlighting, as one might expect, that the overall rate of RO<sub>2</sub>  
420 isomerisation is variable and likely depends on the specific RO<sub>2</sub> species present at a particular time or location. In the PRD  
study (Tan et al., 2019), the HO<sub>2</sub> budget was closed when  $\alpha = 0.95$  was used suggesting that acyl peroxy radicals and those  
derived from long-chain alkanes and monoterpenes only made up a very small fraction of the total RO<sub>2</sub> concentration.

Although revealing, this type of experimental budget analysis coupled with the radical observations is unable to differentiate  
425 between different RO<sub>2</sub> types and so assumptions have to be made on the fraction of the total RO<sub>2</sub> that propagate to HO<sub>2</sub>. In the  
following section, a box model constrained to the latest MCM scheme (MCM3.3.1) is used to predict the radical concentrations.  
The MCM is a near explicit model and, as such, treats the production, propagation and destruction of each RO<sub>2</sub> species present  
discretely and so can provide an insight into the rate at which different RO<sub>2</sub> species convert to HO<sub>2</sub> or to other RO<sub>2</sub> species  
(or, indeed to OH) and the impact this propagation has on NO to NO<sub>2</sub> conversion and, hence, O<sub>3</sub> production.

430

### 3.4 MCM modelled radical predictions and comparison with observations

The time-series of the model-predicted radical concentrations and a breakdown of the modelled OH reactivity from the base  
MCM model are overlaid with the observations in figure 2. The average diurnal of the measured and modelled radical and  
k(OH) profiles are also provided in figure 5. In contrast to the experimental budget analysis, the model predicted OH is in  
435 excellent agreement with the observed OH throughout the campaign. This same model over-estimates HO<sub>2</sub>, however,  
particularly during the daytime, but also during the evening when a small secondary peak in HO<sub>2</sub> is predicted but not observed.  
An exception to this trend occurs between the 9<sup>th</sup> – 12<sup>th</sup> June when elevated levels of NO were measured at the site during the  
day and on these days, the agreement between the observed HO<sub>2</sub> and the model is better. The over-prediction of HO<sub>2</sub> primarily  
occurs under the lower NO conditions that were typically observed during the afternoon hours; the skill of the model to predict  
440 the radical concentrations as a function of NO is discussed further below. The model under-estimates total RO<sub>2</sub> throughout the  
measurement period, although the level of disagreement (in absolute concentration) is most severe from the 15<sup>th</sup> – 22<sup>nd</sup> June  
when NO concentrations were at their lowest. During this period, the observed RO<sub>2</sub> concentrations were most elevated relative  
to other times during the campaign, however, the model does not predict a similar increase in RO<sub>2</sub> concentrations during this



period relative to other times in the campaign. OH reactivity is under-estimated by the model, on average by  $\sim 10 \text{ s}^{-1}$ . However, between the 15<sup>th</sup> – 22<sup>nd</sup> June the average missing OH reactivity increases to  $\sim 13 \text{ s}^{-1}$ . The model underestimation of OH reactivity may, in part, contribute to the model under-estimation of  $\text{RO}_2$  as the model is evidently underestimating the rate of OH + VOC reactions which form  $\text{RO}_2$ . Including an additional reaction between OH and VOC to account for the missing reactivity in the model and the impact this has on the modelled radical concentrations is investigated in section 3.6. Although the model is able to capture the observed OH concentrations reasonably well, the model's failure to reproduce the observed  $\text{HO}_2$  and  $\text{RO}_2$  (and in the base model, the OH reactivity) indicates the model is either missing or misrepresenting some key reactions. Furthermore, the discrepancy between the model-predicted OH and OH budget analysis which highlighted a missing OH source, suggests that the over-prediction of  $\text{HO}_2$  is masking a missing OH source in the MCM model.

Qualitatively, the model over-estimation of  $\text{HO}_2$  and under-estimation of  $\text{RO}_2$  is consistent with the budget analysis which identified a missing  $\text{RO}_2$  production term and missing  $\text{HO}_2$  destruction term which could be reconciled, in part, by slowing the rate at which  $\text{RO}_2$  propagate to  $\text{HO}_2$ . However, when the  $\text{HO}_2$  measured to modelled ratio is binned against NO, differences between the model and budget analyses become apparent (figure 6). The model over-predicts the observed  $\text{HO}_2$  concentrations at the lowest NO mixing ratios experienced ( $0.1 - 1 \text{ ppbv}$ ); this over-prediction can be reconciled (under the very lowest NO conditions,  $<0.3 \text{ ppbv}$ ) when a loss of  $\text{HO}_2$  to aerosols (calculated using Eq. 9, with an uptake coefficient of 0.2) is included in the model. This demonstrates that a reduction in aerosol surface area has the potential to enhance  $\text{HO}_2$  concentrations and thereby increase photochemical ozone formation, but only under very low NO conditions. As there was little to no change in the modelled  $\text{HO}_2$  concentration upon inclusion of an heterogeneous loss term under the higher NO conditions, efforts to reduce anthropogenic PM when NO is present (which is highly likely to be the case) would not be expected to lead to an increase in  $\text{HO}_2$  and, in turn,  $\text{O}_3$  as was suggested from earlier modelling studies (Li et al., 2019). Between  $1 - 5 \text{ ppbv}$  NO, the model is able to reproduce the observed  $\text{HO}_2$  well (between the 9<sup>th</sup> – 12<sup>th</sup> June, the daytime NO concentrations fell within this intermediate NO range, hence the good agreement between the model and observations on these days). In contrast with the budget analysis, the model under-predicts  $\text{HO}_2$  beyond  $5 \text{ ppbv}$  NO by up to a factor of 10 at the highest NO experienced (see the  $52 \text{ ppbv}$  NO bin, figure 6, which includes NO mixing ratios up to  $104 \text{ ppbv}$ ). The model under-predicts the observed  $\text{RO}_2$  over the whole NO range and, consistent with the  $\text{RO}_2$  budget analysis, the under-prediction (in terms of %) is greatest at the highest NO concentrations experienced during the morning hours. The model under-predicts the observed  $\text{RO}_2$  by  $\sim$ factor of 70 in the highest NO mixing ratio bin-range whereas the destruction rate of  $\text{RO}_2$  exceeded the production rate by a factor of  $\sim 10$  in the budget analysis. This large under-prediction of  $\text{RO}_2$  by the model under the highest NO concentrations is most likely driving the differences noted between the P to D( $\text{HO}_2$ ) and the measured to modelled ( $\text{HO}_2$ ) ratios at NO mixing ratios  $>5 \text{ ppbv}$ . Previous radical studies made at urban sites which were influenced by a range of  $\text{NO}_x$  concentrations have demonstrated that the level of agreement between model predictions and the observations tends to vary with the level of NO: Models have a tendency to under-predict the observed OH concentrations at NO mixing ratios below  $1 \text{ ppbv}$  (Lu et al., 2012; Lu et al., 2013; Tan et al., 2017; Whalley et al., 2018) and  $\text{RO}_2$  concentrations are increasingly under-predicted as NO concentrations rise (Tan et al., 2017; Whalley et al., 2018; Slater et al., 2020).



Cl atoms, formed from the photolysis of nitryl chloride (CINO<sub>2</sub>) have been shown to act as a source of RO<sub>2</sub> (Riedel et al., 2014; Bannan et al., 2015; Tan et al., 2017) and have also been investigated here to see if Cl chemistry can resolve the modelled  
480 RO<sub>2</sub> under-prediction under the elevated NO concentrations which were typically observed during the mornings. CINO<sub>2</sub> was measured for part of the campaign (Zhou et al., 2018) and reached up to 1.44 ppbv during the night on the 12<sup>th</sup> – 13<sup>th</sup> June. The Cl atom concentration, calculated from the concentration of CINO<sub>2</sub>, its photolysis rate to yield Cl (determined from the observed actinic flux and published absorption cross section of CINO<sub>2</sub>) and the VOC loading, exceeded 4 × 10<sup>4</sup> atoms cm<sup>-3</sup> during the morning of the 13<sup>th</sup> June and exceeded 1 × 10<sup>4</sup> atoms cm<sup>-3</sup> on several other mornings (figure 7). During these times,  
485 the modelled RO<sub>2</sub> concentrations increased, relative to the concentration in the base model, by up to 2.5 × 10<sup>8</sup> molecule cm<sup>-3</sup> which represents close to a 100% increase in the modelled RO<sub>2</sub> at these times. On several mornings (4<sup>th</sup>, 5<sup>th</sup>, 7<sup>th</sup> and 13<sup>th</sup> June) this increase in RO<sub>2</sub> brought the model and measured RO<sub>2</sub> into close agreement. The production rate of RO<sub>2</sub> from Cl-initiated VOC oxidation on these mornings would serve to enhance P(RO<sub>x</sub>) to the rate of D(RO<sub>x</sub>). However, on several nights, only low concentrations of CINO<sub>2</sub> were measured and only very low concentrations of Cl atoms were calculated to be present upon  
490 sunrise and so, on these days, only modest enhancements (1 – 2 × 10<sup>7</sup> molecule cm<sup>-3</sup>) in RO<sub>2</sub> concentrations were predicted by the model and the large under-prediction in the RO<sub>2</sub> concentration on these mornings remained which may indicate that there are other, overlooked, primary RO<sub>x</sub> sources in the experimental budget calculation besides missing Cl + VOC reactions. The Cl atom concentration dropped off rapidly during the mornings with just ~100 atoms cm<sup>-3</sup> present by noon on most days and so was unable to reconcile the magnitude of the RO<sub>2</sub> underestimation observed throughout the day.

### 495 3.5 Rate of Production and rate of Destruction analysis

A rate of production and rate of destruction analysis on model OH, HO<sub>2</sub> and RO<sub>2</sub> species (figure 8) highlights the main radical sources and sinks in the base model. Consistent with earlier studies of radicals in urban locations, the photolysis of HONO is the dominant primary source of radicals during the daytime, accounting for ~64 % of the primary radical production on average  
500 during the day (05:00 – 19:30) throughout the campaign. The photolysis of O<sub>3</sub> and subsequent reaction of O(<sup>1</sup>D) with H<sub>2</sub>O vapour accounts for ~9 % of primary production during the day, whilst the photolysis of HCHO and other photo-labile VOCs accounts for ~11 % of the radical production. Ozonolysis and nitrate radical (NO<sub>3</sub>) reactions account for 9 % and 7 % of the total radical production during the day, respectively. At night, both ozonolysis (~18 %) and nitrate radical reactions (~82 %) are the source of radicals. The primary source of radicals from VOC+NO<sub>3</sub> reactions is ~ 1 ppbv hr<sup>-1</sup> during the night which is  
505 sufficient to close the RO<sub>x</sub> experimental budget (figure 3).

Figure 9 highlights the rates of propagation in the model which transform OH to HO<sub>2</sub> and RO<sub>2</sub>, RO<sub>2</sub> to HO<sub>2</sub> and HO<sub>2</sub> back to OH. The rate of propagation is rapid and the secondary source of OH from HO<sub>2</sub> + NO is more than twice as large as the primary production of OH from HONO photolysis. Approximately one third of the OH reacts with CO, O<sub>3</sub> or HCHO to form HO<sub>2</sub>, just  
510 over one third reacts with VOCs to form RO<sub>2</sub> and just under one third is lost by reaction with NO<sub>2</sub> forming nitric acid. In



contrast to London (Whalley et al., 2018), the majority of RO<sub>2</sub> formed during AIRPRO propagate to HO<sub>2</sub> and subsequently the majority of HO<sub>2</sub> propagates back to OH. From the model radical flux analysis, which takes into consideration the different types of RO<sub>2</sub> species present, a value of  $\alpha = 0.87$  is derived (where  $\alpha$  = the rate at which RO forms RO<sub>2</sub> or RC(O)O<sub>2</sub> divided by the rate of RO conversion to HO<sub>2</sub>). Note, this fraction does not consider RO<sub>2</sub> and RC(O)O<sub>2</sub> termination reactions. In London, the model derived  $\alpha$  was  $\sim 0.5$  reflecting the presence of long-chain alkane-derived RO<sub>2</sub> species from diesel emissions and mono-terpenes. In Beijing, measurement of such long-chain VOC species could not be attempted, but these could have been present. A lumped mono-terpene signal was measured by PTR-ToF-MS and is included in the model, split equally between  $\alpha$ -pinene and limonene. The base model, on which the radical flux analysis was performed, under-predicts OH reactivity and so is likely missing RO<sub>2</sub> species from additional OH+VOC reactions which, depending on the RO<sub>2</sub> type may serve to reduce  $\alpha$ .

520

### 3.6 OH reactivity and missing OH reactivity

NO<sub>2</sub> was the single biggest contributor to the OH reactivity in Beijing with a campaign average contribution of 18.6% (figure 5). This is similar to the NO<sub>2</sub> contribution to OH reactivity observed in London (Whalley et al., 2016). NO contributed just 1.3% to the total reactivity in Beijing, compared to a 4.2% contribution in London (Whalley et al., 2016). In London, measured carbonyl species accounted for close to 20% of the OH reactivity budget, largely due to the high concentrations of HCHO (Whalley et al., 2016). In contrast, in Beijing, carbonyls accounted for just 3.8% of the measured  $k(\text{OH})$ . Alkenes and dialkenes were more prevalent in Beijing than in London and the dialkene group of VOCs (dominated by isoprene) accounted for 10.5% of the OH reactivity in Beijing compared to 1.8% in London (Whalley et al., 2016). Owing to the faster physical loss of secondary species in Beijing by ventilation compared to London (see section 2), the contribution that model-generated intermediate species made to the observed OH reactivity was 2.7% in Beijing vs 23.8% in London (Whalley et al., 2016). In contrast to Beijing, where approximately 30% of the measured reactivity remains unaccounted for, in London, the OH reactivity budget was largely closed (Whalley et al., 2016). In Beijing during the measurement period when the missing OH reactivity reached on average  $13 \text{ s}^{-1}$  (15<sup>th</sup> – 22<sup>nd</sup> June), isoprene concentrations were elevated relative to earlier in the campaign (figure 1). Overall, much higher concentrations of isoprene were observed in Beijing than in London (Whalley et al., 2016), and so this may indicate that other biogenic species that were not measured, along with their oxidation products, may account for some of the missing OH reactivity in Beijing.

A series of model simulations have been performed where an additional OH to RO<sub>2</sub> reaction has been included to account for the missing reactivity at a given time (figure 10); the RO<sub>2</sub> formed has been varied to investigate the influence of different RO<sub>2</sub> types on the modelled radical concentrations. When OH converts to methyl peroxy radicals, the modelled RO<sub>2</sub> concentration increases by close to a factor of 2 on average, but just over a factor of 2 under-prediction of the observed RO<sub>2</sub> radicals remains. Unsurprisingly, it is the modelled fraction of RO<sub>2</sub> radicals that do not act as an HO<sub>2</sub> interference (RO<sub>2</sub>-simple) that increase in this scenario and the model now only under-estimates this class of RO<sub>2</sub> species by a factor of 1.45, whilst RO<sub>2</sub>-complex is still under-estimated by a factor of 6.2. When OH converts to HOCH<sub>2</sub>CH<sub>2</sub>O<sub>2</sub> (an RO<sub>2</sub> species that does act as an HO<sub>2</sub> interference,

540



545 formed from the reaction of OH with ethene), the modelled RO<sub>2</sub>-complex fraction increases and the model under-estimation  
of RO<sub>2</sub>-complex is reduced to a factor of 1.8 on average, with the largest under-predictions observed during the evening hours.  
In both these model simulations, the modelled over-prediction of HO<sub>2</sub> increases from the base model scenario as CH<sub>3</sub>O<sub>2</sub> and  
HOCH<sub>2</sub>CH<sub>2</sub>O<sub>2</sub> both rapidly propagate to HO<sub>2</sub>. The modelled OH concentration displays a modest decrease with the additional  
OH sink, however, this is largely compensated for by the increase in modelled HO<sub>2</sub> which enhances the secondary source of  
550 OH from HO<sub>2</sub> + NO, and so, overall, the modelled OH concentration is largely buffered by the inclusion of missing OH  
reactivity in the form of additional methane (leading to CH<sub>3</sub>O<sub>2</sub>) or ethene (leading to HOCH<sub>2</sub>CH<sub>2</sub>O<sub>2</sub>)

Model simulations (not shown) which include an additional source of CH<sub>3</sub>C(O)O<sub>2</sub>, for example, from additional CH<sub>3</sub>CHO+OH  
reactions, do predict substantially less HO<sub>2</sub> (and can reconcile the observed HO<sub>2</sub> to within 25%), but modelled RO<sub>2</sub>  
555 concentrations do not increase as a large fraction of the acyl-RO<sub>2</sub> radicals react with NO<sub>2</sub> to form PAN and are, therefore, lost.  
These missing reactivity model simulations and measurement comparisons suggest that the missing RO<sub>2</sub> may be a species  
which, upon reaction with NO, converts from one RO<sub>2</sub> species to another and, therefore, compete with RO<sub>2</sub> to HO<sub>2</sub> propagation  
rather than a RO<sub>2</sub> radical which lead to RO<sub>2</sub> termination. This suggests that the overall lifetime of RO<sub>2</sub> radicals is longer than  
currently estimated and that multiple conversions of one RO<sub>2</sub> species to another may be occurring to sustain the high  
560 concentrations observed. As identified in London, larger, more complex VOC species such as mono-terpenes or long-chain  
alkanes deriving from diesel emissions do undergo multiple RO<sub>2</sub> to RO<sub>2</sub> conversions in the presence of NO as the alkoxy  
radical formed preferentially undergoes isomerisation rather than an external H atom abstraction by O<sub>2</sub>. If an additional reaction  
which converts OH to an RO<sub>2</sub> species formed during the oxidation of α-pinene, and which undergoes four reactions with NO  
before eventually forming HO<sub>2</sub>, is added to the model at a rate sufficient to reconcile the missing OH reactivity, the model  
565 predicts significantly more total RO<sub>2</sub> and now only modestly under-predicts the observed RO<sub>2</sub> concentrations (by a factor of  
1.8). In this simulation, both the simple- and complex-RO<sub>2</sub> species are enhanced, as the first 3 generations of RO<sub>2</sub> species  
formed would be detected during the RO<sub>x</sub>-mode in the RO<sub>x</sub>-LIF instrument and, hence, contribute to RO<sub>2</sub>-simple. The final  
RO<sub>2</sub> species formed, that does propagate to HO<sub>2</sub> via RO upon reaction with NO, would be detected during the HO<sub>x</sub>-mode in  
the RO<sub>x</sub>LIF instrument and, as such, contributes to the RO<sub>2</sub>-complex fraction. In this scenario, the HO<sub>2</sub> concentration is now  
570 only modestly over-estimated by a factor of 1.4. The RO<sub>x</sub>LIF instrument relies on the conversion of RO<sub>2</sub> species to HO<sub>2</sub> (and  
ultimately to OH) for detection, so one might expect the instrument to be insensitive to RO<sub>2</sub> species that do not directly  
propagate to RO then to HO<sub>2</sub> upon reaction with NO. However, given the RO<sub>x</sub>LIF flow tube conditions (NO concentration of  
4 × 10<sup>13</sup> molecule cm<sup>-3</sup> and residence time of just under 1 s) RO<sub>2</sub> species that require several reactions with NO before HO<sub>2</sub> is  
produced should still be detected. These types of RO<sub>2</sub> species that require more than one reaction with NO before HO<sub>2</sub> forms  
575 may be generated via the additional VOC+OH reactions identified as missing OH reactivity (as presented here). They may  
also be present due to a missing primary source of RO<sub>2</sub> such as decomposition of a complex PAN species, VOC photolysis, a  
Cl atom + VOC reaction or an alkene ozonolysis product. The experimental peroxy radical budget analysis highlighted that  
budget closure could only be achieved if α was reduced to 0.1, which suggests that the model breakdown of peroxy radical



species present (e.g. the fraction of acyl-RO<sub>2</sub>, long- vs short-chained alkyl-RO<sub>2</sub> species) may be incomplete. In the scenario  
580 where OH converts to an  $\alpha$ -pinene-derived RO<sub>2</sub> species, consistent with the experimental budget analysis, the model under-  
predicts the observed OH by a factor of 1.8 revealing that there is a missing source of OH under the low NO conditions in  
Beijing that was previously masked by the model over-prediction of HO<sub>2</sub>.

### 3.7 Impact on ozone production

585

Previous work, for example, by Tan et al (2017), suggested that the addition of a primary RO<sub>2</sub> source could help reconcile the  
model under-prediction of RO<sub>2</sub>. However, as demonstrated in section 3.6, the identity of the primary RO<sub>2</sub> is important and in  
Beijing a complex RO<sub>2</sub> species that has a large enough carbon skeleton such that the RO radical formed upon reaction with  
NO preferentially isomerises to another RO<sub>2</sub> (and undergoes multiple RO<sub>2</sub> to RO<sub>2</sub> conversions before *eventually* forming HO<sub>2</sub>)  
590 is needed to reconcile both the observed RO<sub>2</sub> and HO<sub>2</sub> concentrations. These types of RO<sub>2</sub> species may also preferentially  
isomerise rather than undergo the bimolecular reactions with NO if NO concentrations are low enough. For example, laboratory  
studies have shown that the monoterpenes, following an initial attack by ozone or OH, form highly oxidised RO<sub>2</sub> radicals  
within a few seconds via repeated H-shift from C–H to an R–O–O bond and subsequent O<sub>2</sub> additions (Jokinen et al., 2014;  
Ehn et al., 2014; Berndt et al., 2016). Recently, autoxidation has also been shown to occur during the oxidation of aromatic  
595 VOCs too (Wang et al., 2017b). Autoxidation reactions may generate OH directly from RO<sub>2</sub> and, therefore, may also resolve  
the missing OH source reported under low NO conditions (here and in the literature). These types of autoxidation reactions  
lead to the generation of HOMs also which have been shown to condense and contribute to SOA (Mohr et al., 2019). Mass  
spectrometric signals relating to these highly oxidised RO<sub>2</sub> species were observed during the AIRPRO campaign (Brean et al.,  
2019; Mehra et al., 2020) suggesting that autoxidation was occurring at the Beijing site. Unimolecular H-atom shifts are  
600 represented within the MCM3.3.1 for isoprene oxidation. Autoxidation reactions for other RO<sub>2</sub> radicals are currently not  
included within the MCM3.3.1, although improved representation of RO<sub>2</sub> radical chemistry is a focus for the next generation  
of explicit detailed chemical mechanisms (Jenkin et al., 2019).

The model measurement comparisons above suggest that our understanding of the rate at which the larger RO<sub>2</sub> species  
propagate to HO<sub>2</sub> (or to OH directly) and the possible reactions they undergo (which have not undergone substantial laboratory  
605 study) is far from complete and highlights that RO<sub>2</sub> chemistry warrants further study. One important finding, however, is that  
the underestimation of the observed RO<sub>2</sub> may be caused by missing reactions that compete with the RO<sub>2</sub>+NO reactions that  
form HO<sub>2</sub>. These competing reactions are effectively slowing the rate at which RO<sub>2</sub> species convert to HO<sub>2</sub>, but if, as suggested  
here, these reactions are RO<sub>2</sub>+NO reactions that reform another RO<sub>2</sub> radical, they will still be relevant in terms of ozone  
production. Under low NO conditions there is emerging evidence that unimolecular isomerisation reactions occur for a range  
610 of RO<sub>2</sub> radicals (Jokinen et al., 2014; Ehn et al., 2014; Berndt et al., 2016; Wang et al., 2017b); these reactions will effectively



remove RO<sub>2</sub> radicals without conversion of NO to NO<sub>2</sub> and so also have implications for modelling in situ O<sub>3</sub> production, if models rely only on the rate of VOC oxidation when investigating O<sub>3</sub> production.

By approximating the rate of ozone production to the rate of NO<sub>2</sub> production from the reaction of NO with HO<sub>2</sub> and RO<sub>2</sub> radicals, urban radical measurements can be used to estimate local ozone formation (Kanaya et al., 2007; Ren et al., 2013; 615 Brune et al., 2016; Tan et al., 2017; Whalley et al., 2018). Losses of NO<sub>2</sub> that do not yield O<sub>3</sub>, for example through nitric acid and PAN formation, need to be estimated and then subtracted:

$$P(\text{O}_3) = (k_{\text{HO}_2+\text{NO}}[\text{HO}_2][\text{NO}] + k_{\text{RO}_2+\text{NO}}[\text{RO}_2][\text{NO}]) - (k_{\text{OH}+\text{NO}_2+\text{M}}[\text{OH}][\text{NO}_2][\text{M}] + k_{\text{RO}_2+\text{NO}_2+\text{M}}[\text{RO}_2][\text{NO}_2][\text{M}]) \quad (11)$$

Using this approach, recent studies where OH, HO<sub>2</sub> and RO<sub>2</sub> observations (via RO<sub>x</sub>LIF) were made, demonstrated that models 620 may under-predict ozone production at high NO due to an underestimation of the RO<sub>2</sub> radical concentrations at high NO concentrations (Tan et al., 2017; Whalley et al., 2018). Figure 11 displays the mean ozone production calculated from the radical observations (red line) as a function of NO and, consistent with the earlier ozone production calculations from the Wangdu (Tan et al., 2017) and London (Whalley et al., 2018) studies, the in situ ozone production calculated from the modelled OH and peroxy radicals (black line) is lower than from the observed radicals, most significantly at the higher NO 625 concentrations. To accurately simulate ozone production and to understand how emission reduction policies may impact ozone levels, it is essential that the model accurately reflects the types of RO<sub>2</sub> species present and how fast they propagate to another RO<sub>2</sub> species, or to HO<sub>2</sub> or to OH.

## 5 Conclusions

Measurement and model comparisons of OH, HO<sub>2</sub>, RO<sub>2</sub>-complex, RO<sub>2</sub>-simple and total RO<sub>2</sub> in Beijing have displayed varying 630 levels of agreement as a function of NO<sub>x</sub>. Under low NO conditions, consistent with previous studies in low NO<sub>x</sub> but high VOC environments, a missing OH source is evident. Radical budget analysis has demonstrated that this missing OH source could be resolved if unimolecular reactions of RO<sub>2</sub> radicals generate OH directly. Under the low NO conditions (< 1 ppbv), the MCM over-predicted HO<sub>2</sub>, although this over-prediction could be resolved at very low NO mixing ratios (<0.3 ppbv) by including a heterogeneous loss term to aerosol surfaces. This highlights that a reduction in aerosol surface area has the potential 635 to enhance HO<sub>2</sub> concentrations and thereby increase photochemical ozone formation, but only under very low NO conditions. The model under-predicted RO<sub>2</sub>, most severely under high NO conditions (>1 ppbv). Although Cl atoms could increase the concentration of RO<sub>2</sub>, this enhancement was limited to times when the Cl atom concentration was elevated and could not resolve the RO<sub>2</sub> under-prediction observed at all times. In the presence of NO, the model over-estimates the rate at which RO<sub>2</sub> propagates to HO<sub>2</sub> and we hypothesise that larger RO<sub>2</sub> species likely undergo multiple bimolecular reactions with NO,



640 followed by isomerisation of the RO radical to another RO<sub>2</sub> species, before a HO<sub>2</sub> radical forms. By this process, the lifetime  
and the concentration of total-RO<sub>2</sub> radicals is extended. The ozone production efficiency of large, complex VOCs from which  
these RO<sub>2</sub> species are formed may be greater than currently appreciated, and so further efforts to understand the rate at which  
the larger RO<sub>2</sub> species propagate to HO<sub>2</sub> (or to OH directly) and all the possible reactions they undergo, is necessary to  
accurately model ozone levels in urban centres such as Beijing and to fully understand how emission controls will impact  
645 ozone.

**Data availability.** Data presented in this study are available from the author upon request (l.k.whalley@leeds.ac.uk).

**Author contributions.** LW, ES, RWM, CY and DH carried out the measurements; LW and ES developed the model and  
performed the calculations; JL, FS, JH, RD, MS, JH, AL, AM, SW, AB, TB, HC, BO, RJ, LC, LK, WB, TV, SK, SG, YS,  
WX, SY, LR, WA, CH, XW and PF provided logistical support and supporting data to constrain the model; LW prepared the  
650 manuscript, with contributions from all the co-authors.

**Competing interests.** The authors declare that they have no conflict of interest.

**Acknowledgements** – We are grateful to the Natural Environment Research Council for funding via the Newton Fund  
Atmospheric Pollution and Human Health in Chinese Megacity Directed International Program (grant number NE/N006895/1)  
and the National Natural Science Foundation of China (Grant No.41571130031). Eloise Slater, Freya Squires and Archit Mehra  
655 acknowledge NERC SPHERES PhD studentships. We would like to thank Likun Xue and co-authors for the providing the  
chlorine chemistry module used in the MCM. We acknowledge the support from Zifa Wang and Jie Li from the Institute of  
Applied Physics (IAP), Chinese Academy of Sciences for hosting the APHH-Beijing campaign. We thank Liangfang Wei,  
Hong Ren, Qiaorong Xie, Wanyu Zhao, Linjie Li, Ping Li, Shengjie Hou and Qingqing Wang from IAP, Kebin He and  
Xiaoting Cheng from Tsinghua University, and James Allan from the University of Manchester for providing logistic and  
660 scientific support for the field campaigns. We would also like to thank other participants in the APHH field campaign.

## References

Bannan, T. J., Booth, A. M., Bacak, A., Muller, J. B. A., Leather, K. E., Le Breton, M., Jones, B., Young, D., Coe, H., Allan,  
J., Visser, S., Slowik, J. G., Furger, M., Prevot, A. S. H., Lee, J., Dunmore, R. E., Hopkins, J. R., Hamilton, J. F., Lewis, A.  
C., Whalley, L. K., Sharp, T., Stone, D., Heard, D. E., Fleming, Z. L., Leigh, R., Shallcross, D. E., and Percival, C. J.: The  
665 first UK measurements of nitryl chloride using a chemical ionization mass spectrometer in central London in the summer of



- 2012, and an investigation of the role of Cl atom oxidation, *J Geophys Res-Atmos*, 120, 5638-5657, 10.1002/2014JD022629, 2015.
- Berndt, T., Richters, S., Jokinen, T., Hyttinen, N., Kurten, T., Otkjaer, R. V., Kjaergaard, H. G., Stratmann, F., Herrmann, H., Sipila, M., Kulmala, M., and Ehn, M.: Hydroxyl radical-induced formation of highly oxidized organic compounds, *Nat Commun*, 7, Artn 13677 10.1038/Ncomms13677, 2016.
- Bigi, A., and Harrison, R. M.: Analysis of the air pollution climate at a central urban background site, *Atmos Environ*, 44, 2004-2012, 10.1016/j.atmosenv.2010.02.028, 2010.
- Brean, J., Harrison, R. M., Shi, Z. B., Beddows, D. C. S., Acton, W. J. F., Hewitt, C. N., Squires, F. A., and Lee, J.: Observations of highly oxidized molecules and particle nucleation in the atmosphere of Beijing, *Atmos Chem Phys*, 19, 14933-14947, 10.5194/acp-19-14933-2019, 2019.
- Brune, W. H., Baier, B. C., Thomas, J., Ren, X., Cohen, R. C., Pusede, S. E., Browne, E. C., Goldstein, A. H., Gentner, D. R., Keutsch, F. N., Thornton, J. A., Harrold, S., Lopez-Hilfiker, F. D., and Wennberg, P. O.: Ozone production chemistry in the presence of urban plumes, *Faraday Discuss*, 189, 169-189, 10.1039/c5fd00204d, 2016.
- Chatani, S., Shimo, N., Matsunaga, S., Kajii, Y., Kato, S., Nakashima, Y., Miyazaki, K., Ishii, K., and Ueno, H.: Sensitivity analyses of OH missing sinks over Tokyo metropolitan area in the summer of 2007, *Atmos Chem Phys*, 9, 8975-8986, DOI 10.5194/acp-9-8975-2009, 2009.
- Chen, R. J., Zhao, Z. H., and Kan, H. D.: Heavy Smog and Hospital Visits in Beijing, China, *Am J Resp Crit Care*, 188, 1170-1171, DOI 10.1164/rccm.201304-0678LE, 2013.
- Commane, R., Floquet, C. F. A., Ingham, T., Stone, D., Evans, M. J., and Heard, D. E.: Observations of OH and HO<sub>2</sub> radicals over West Africa, *Atmos Chem Phys*, 10, 8783-8801, 10.5194/acp-10-8783-2010, 2010.
- Crilly, L. R., Kramer, L. J., Ouyang, B., Duan, J., Zhang, W. Q., Tong, S. R., Ge, M. F., Tang, K., Qin, M., Xe, P. H., Shaw, M., Lewis, A. C., Mehra, A., Bannan, T. J., Worrall, S. D., Priestley, M., Bacak, A., Coe, H., Allan, J., Percival, C. J., Popoola, O. A. M., Jones, R. L., and Bloss, W. J.: Intercomparison of nitrous acid (HONO) measurement techniques in a megacity (Beijing), *Atmos Meas Tech*, 12, 6449-6463, 10.5194/amt-12-6449-2019, 2019.
- Cryer, D. R.: Measurements of hydroxyl radical reactivity and formaldehyde in the atmosphere, PhD, School of Chemistry, University of Leeds, UK, 2016.
- Ehn, M., Thornton, J. A., Kleist, E., Sipila, M., Junninen, H., Pullinen, I., Springer, M., Rubach, F., Tillmann, R., Lee, B., Lopez-Hilfiker, F., Andres, S., Acir, I. H., Rissanen, M., Jokinen, T., Schobesberger, S., Kangasluoma, J., Kontkanen, J., Nieminen, T., Kurten, T., Nielsen, L. B., Jorgensen, S., Kjaergaard, H. G., Canagaratna, M., Dal Maso, M., Berndt, T., Petaja, T., Wahner, A., Kerminen, V. M., Kulmala, M., Worsnop, D. R., Wildt, J., and Mentel, T. F.: A large source of low-volatility secondary organic aerosol, *Nature*, 506, 476-+, 10.1038/nature13032, 2014.
- Fuchs, H., Holland, F., and Hofzumahaus, A.: Measurement of tropospheric RO<sub>2</sub> and HO<sub>2</sub> radicals by a laser-induced fluorescence instrument, *Rev Sci Instrum*, 79, Artn 084104 10.1063/1.2968712, 2008.



- Fuchs, H., Tan, Z. F., Lu, K. D., Bohn, B., Broch, S., Brown, S. S., Dong, H. B., Gomm, S., Haseler, R., He, L. Y.,  
700 Hofzumahaus, A., Holland, F., Li, X., Liu, Y., Lu, S. H., Min, K. E., Rohrer, F., Shao, M., Wang, B. L., Wang, M., Wu, Y.  
S., Zeng, L. M., Zhang, Y. S., Wahner, A., and Zhang, Y. H.: OH reactivity at a rural site (Wangdu) in the North China  
Plain: contributions from OH reactants and experimental OH budget, *Atmos Chem Phys*, 17, 645-661, 10.5194/acp-17-645-  
2017, 2017.
- He, H., Liang, X. Z., Sun, C., Tao, Z. N., and Tong, D. Q.: The long-term trend and production sensitivity change in the US  
705 ozone pollution from observations and model simulations, *Atmos Chem Phys*, 20, 3191-3208, 10.5194/acp-20-3191-2020,  
2020.
- Hofzumahaus, A., Rohrer, F., Lu, K. D., Bohn, B., Brauers, T., Chang, C. C., Fuchs, H., Holland, F., Kita, K., Kondo, Y., Li,  
X., Lou, S. R., Shao, M., Zeng, L. M., Wahner, A., and Zhang, Y. H.: Amplified Trace Gas Removal in the Troposphere,  
*Science*, 324, 1702-1704, 10.1126/science.1164566, 2009.
- 710 Hopkins, J. R., Jones, C. E., and Lewis, A. C.: A dual channel gas chromatograph for atmospheric analysis of volatile  
organic compounds including oxygenated and monoterpene compounds, *Journal of Environmental Monitoring*, 13, 2268-  
2276, 2011.
- Huang, J., Pan, X. C., Guo, X. B., and Li, G. X.: Health impact of China's Air Pollution Prevention and Control Action Plan:  
an analysis of national air quality monitoring and mortality data, *Lancet Planet Health*, 2, E313-E323, Doi 10.1016/S2542-  
715 5196(18)30141-4, 2018.
- Huang, R. J., Zhang, Y. L., Bozzetti, C., Ho, K. F., Cao, J. J., Han, Y. M., Daellenbach, K. R., Slowik, J. G., Platt, S. M.,  
Canonaco, F., Zotter, P., Wolf, R., Pieber, S. M., Bruns, E. A., Crippa, M., Ciarelli, G., Piazzalunga, A., Schwikowski, M.,  
Abbaszade, G., Schnelle-Kreis, J., Zimmermann, R., An, Z. S., Szidat, S., Baltensperger, U., El Haddad, I., and Prevot, A. S.  
H.: High secondary aerosol contribution to particulate pollution during haze events in China, *Nature*, 514, 218-222,  
720 10.1038/nature13774, 2014.
- Huang, Z., Zhang, Y., Yan, Q., Zhang, Z., and Wang, X.: Real-time monitoring of respiratory absorption factors of volatile  
organic compounds in ambient air by proton transfer reaction time-of-flight mass spectrometry, *Journal of hazardous  
materials*, 320, 547-555, 2016.
- Jacob, D. J.: Heterogeneous chemistry and tropospheric ozone, *Atmos Environ*, 34, 2131-2159, Doi 10.1016/S1352-  
725 2310(99)00462-8, 2000.
- Jenkin, M. E., Young, J. C., and Rickard, A. R.: The MCM v3.3.1 degradation scheme for isoprene, *Atmos Chem Phys*, 15,  
11433-11459, 10.5194/acp-15-11433-2015, 2015.
- Jenkin, M. E., Valorso, R., Aumont, B., and Rickard, A. R.: Estimation of rate coefficients and branching ratios for reactions  
of organic peroxy radicals for use in automated mechanism construction, *Atmos Chem Phys*, 19, 7691-7717, 10.5194/acp-  
730 19-7691-2019, 2019.



- Jokinen, T., Sipila, M., Richters, S., Kerminen, V. M., Paasonen, P., Stratmann, F., Worsnop, D., Kulmala, M., Ehn, M., Herrmann, H., and Berndt, T.: Rapid Autoxidation Forms Highly Oxidized RO<sub>2</sub> Radicals in the Atmosphere, *Angew Chem Int Edit*, 53, 14596-14600, 10.1002/anie.201408566, 2014.
- 735 Kanaya, Y., Cao, R. Q., Akimoto, H., Fukuda, M., Komazaki, Y., Yokouchi, Y., Koike, M., Tanimoto, H., Takegawa, N., and Kondo, Y.: Urban photochemistry in central Tokyo: 1. Observed and modeled OH and HO<sub>2</sub> radical concentrations during the winter and summer of 2004, *J Geophys Res-Atmos*, 112, Artn D21312 10.1029/2007jd008670, 2007.
- Kotthaus, S. and Grimmond, C. S. B.: Atmospheric boundary layer characteristics from ceilometer measurements part 1: A new method to track mixed layer height and classify clouds, *Q. J. Roy. Meteorol. Soc.*, 144, 1525–1538, <https://doi.org/10.1002/qj.3299>, 2018.
- 740 Li, K., Jacob, D. J., Liao, H., Shen, L., Zhang, Q., and Bates, K. H.: Anthropogenic drivers of 2013-2017 trends in summer surface ozone in China, *P Natl Acad Sci USA*, 116, 422-427, 10.1073/pnas.1812168116, 2019.
- Lou, S., Holland, F., Rohrer, F., Lu, K., Bohn, B., Brauers, T., Chang, C. C., Fuchs, H., Haseler, R., Kita, K., Kondo, Y., Li, X., Shao, M., Zeng, L., Wahner, A., Zhang, Y., Wang, W., and Hofzumahaus, A.: Atmospheric OH reactivities in the Pearl River Delta - China in summer 2006: measurement and model results, *Atmos Chem Phys*, 10, 11243-11260, 10.5194/acp-745 10-11243-2010, 2010.
- Lu, K. D., Rohrer, F., Holland, F., Fuchs, H., Bohn, B., Brauers, T., Chang, C. C., Haseler, R., Hu, M., Kita, K., Kondo, Y., Li, X., Lou, S. R., Nehr, S., Shao, M., Zeng, L. M., Wahner, A., Zhang, Y. H., and Hofzumahaus, A.: Observation and modelling of OH and HO<sub>2</sub> concentrations in the Pearl River Delta 2006: a missing OH source in a VOC rich atmosphere, *Atmos Chem Phys*, 12, 1541-1569, 10.5194/acp-12-1541-2012, 2012.
- 750 Lu, K. D., Hofzumahaus, A., Holland, F., Bohn, B., Brauers, T., Fuchs, H., Hu, M., Haseler, R., Kita, K., Kondo, Y., Li, X., Lou, S. R., Oebel, A., Shao, M., Zeng, L. M., Wahner, A., Zhu, T., Zhang, Y. H., and Rohrer, F.: Missing OH source in a suburban environment near Beijing: observed and modelled OH and HO<sub>2</sub> concentrations in summer 2006, *Atmos Chem Phys*, 13, 1057-1080, 10.5194/acp-13-1057-2013, 2013.
- Lu, K. D., Rohrer, F., Holland, F., Fuchs, H., Brauers, T., Oebel, A., Dlugi, R., Hu, M., Li, X., Lou, S. R., Shao, M., Zhu, T., 755 Wahner, A., Zhang, Y. H., and Hofzumahaus, A.: Nighttime observation and chemistry of HO<sub>x</sub> in the Pearl River Delta and Beijing in summer 2006, *Atmos Chem Phys*, 14, 4979-4999, 10.5194/acp-14-4979-2014, 2014.
- Lu, K. D., Guo, S., Tan, Z. F., Wang, H. C., Shang, D. J., Liu, Y. H., Li, X., Wu, Z. J., Hu, M., and Zhang, Y. H.: Exploring atmospheric free-radical chemistry in China: the self-cleansing capacity and the formation of secondary air pollution, *Natl Sci Rev*, 6, 579-594, 10.1093/nsr/nwy073, 2019.
- 760 Mao, J. Q., Ren, X. R., Chen, S. A., Brune, W. H., Chen, Z., Martinez, M., Harder, H., Lefer, B., Rappengluck, B., Flynn, J., and Leuchner, M.: Atmospheric oxidation capacity in the summer of Houston 2006: Comparison with summer measurements in other metropolitan studies, *Atmos Environ*, 44, 4107-4115, 10.1016/j.atmosenv.2009.01.013, 2010.
- Martinez, M., Harder, H., Kovacs, T. A., Simpas, J. B., Bassis, J., Leshner, R., Brune, W. H., Frost, G. J., Williams, E. J., Stroud, C. A., Jobson, B. T., Roberts, J. M., Hall, S. R., Shetter, R. E., Wert, B., Fried, A., Alicke, B., Stutz, J., Young, V. L.,



- 765 White, A. B., and Zamora, R. J.: OH and HO<sub>2</sub> concentrations, sources, and loss rates during the Southern Oxidants Study in Nashville, Tennessee, summer 1999, *J Geophys Res-Atmos*, 108, Artn 4617 10.1029/2003jd003551, 2003.
- Mehra, A., Canagaratna, M., Bannan, T., Worrall, S. D., Bacak, A., Priestley, M., Zhao, J., Xu, W., Wang, Y., Cheng, X., Wang, L., Hamilton, J., Chen, Q., Stark, H., Krechmer, J. E., Squires, F. A., Lee, J., Brean, J., Slater, E. J., Whalley, L. K., Heard, D. E., Ouyang, B., Acton, W. J., Hewitt, C. N., Wang, X., Liu, D., Jayne, J. T., Sun, Y., Fu, P., Worsnop, D., Allan, J., Percival, C., and Coe, H.: Using highly time-resolved online mass spectrometry to examine biogenic and anthropogenic contributions to organic aerosol in Beijing *Faraday Discuss*, 2020.
- 770 Michoud, V., Kukui, A., Camredon, M., Colomb, A., Borbon, A., Miet, K., Aumont, B., Beekmann, M., Durand-Jolibois, R., Perrier, S., Zapf, P., Siour, G., Ait-Helal, W., Locoge, N., Sauvage, S., Afif, C., Gros, V., Furger, M., Ancellet, G., and Doussin, J. F.: Radical budget analysis in a suburban European site during the MEGAPOLI summer field campaign, *Atmos Chem Phys*, 12, 11951-11974, 10.5194/acp-12-11951-2012, 2012.
- 775 Mohr, C., Thornton, J. A., Heitto, A., Lopez-Hilfiker, F. D., Lutz, A., Riipinen, I., Hong, J., Donahue, N. M., Hallquist, M., Petaja, T., Kulmala, M., and Yli-Juuti, T.: Molecular identification of organic vapors driving atmospheric nanoparticle growth, *Nat Commun*, 10, Artn 4442 10.1038/S41467-019-12473-2, 2019.
- Newland, M. J., Bryant, D. J., Dunmore, R., Bannan, T., Acton, W. J., Langford, B., Hopkins, J., Squires, F. A., Dixon, W. J., Drysdale, W. S., Ivatt, P. D., Evans, M. J., Edwards, P., Whalley, L. K., Heard, D. E., Slater, E. J., Woodward-Massey, R., Ye, C., Mehra, A., Worrall, S. D., Bacak, A., Coe, H., Percival, C., Hewitt, C. N., Lee, J. D., Cui, T. Q., Surratt, J. D., Wang, X., Lewis, A. C., Rickard, A. R., and Hamilton, J.: Rainforest-like atmospheric chemistry in a polluted megacity, *Atmospheric Chemistry and Physics Discussions*, 35, 2020.
- 780 Peeters, J., Nguyen, T. L., and Vereecken, L.: HO<sub>x</sub> radical regeneration in the oxidation of isoprene, *Phys Chem Chem Phys*, 11, 5935-5939, 10.1039/b908511d, 2009.
- 785 Peeters, J., Muller, J. F., Stavrou, T., and Nguyen, V. S.: Hydroxyl Radical Recycling in Isoprene Oxidation Driven by Hydrogen Bonding and Hydrogen Tunneling: The Upgraded LIM1 Mechanism, *J Phys Chem A*, 118, 8625-8643, 10.1021/jp5033146, 2014.
- Reeves, C., Mills, G., Whalley, L. K., Acton, W. J., Bloss, W. J., Crilley, L., Grimmond, C. S. B., Heard, D. E., Hewitt, C. N., Hopkins, J., Kotthaus, S., Kramer, L., Jones, R. L., Lee, J. D., Liu, Y., Ouyang, B., Slater, E. J., Squires, F. A., Wang, X., Woodward-Massey, R., and Ye, C.: Observations of speciated isoprene nitrates in Beijing: Implications for isoprene chemistry, *Atmospheric Chemistry and Physics Discussions*, 964, 2019.
- 790 Ren, X. R., Harder, H., Martinez, M., Leshner, R. L., Oligier, A., Shirley, T., Adams, J., Simpasa, J. B., and Brune, W. H.: HO<sub>x</sub> concentrations and OH reactivity observations in New York City during PMTACS-NY2001, *Atmos Environ*, 37, 3627-3637, 10.1016/S1352-2310(03)00460-6, 2003.
- 795 Ren, X. R., van Duin, D., Cazorla, M., Chen, S., Mao, J. Q., Zhang, L., Brune, W. H., Flynn, J. H., Grossberg, N., Lefer, B. L., Rappengluck, B., Wong, K. W., Tsai, C., Stutz, J., Dibb, J. E., Jobson, B. T., Luke, W. T., and Kelley, P.: Atmospheric



- oxidation chemistry and ozone production: Results from SHARP 2009 in Houston, Texas, *J Geophys Res-Atmos*, 118, 5770-5780, 10.1002/jgrd.50342, 2013.
- 800 Riedel, T. P., Wolfe, G. M., Danas, K. T., Gilman, J. B., Kuster, W. C., Bon, D. M., Vlasenko, A., Li, S. M., Williams, E. J., Lerner, B. M., Veres, P. R., Roberts, J. M., Holloway, J. S., Lefer, B., Brown, S. S., and Thornton, J. A.: An MCM modeling study of nitryl chloride (ClNO<sub>2</sub>) impacts on oxidation, ozone production and nitrogen oxide partitioning in polluted continental outflow, *Atmos Chem Phys*, 14, 3789-3800, 10.5194/acp-14-3789-2014, 2014.
- Sadanaga, Y., Yoshino, A., Watanabe, K., Yoshioka, A., Wakazono, Y., Kanaya, Y., and Kajii, Y.: Development of a  
805 measurement system of OH reactivity in the atmosphere by using a laser-induced pump and probe technique, *Rev Sci Instrum*, 75, 2648-2655, 10.1063/1.1775311, 2004.
- Saunders, S. M., Jenkin, M. E., Derwent, R. G., and Pilling, M. J.: Protocol for the development of the Master Chemical Mechanism, MCM v3 (Part A): tropospheric degradation of non-aromatic volatile organic compounds, *Atmos Chem Phys*, 3, 161-180, DOI 10.5194/acp-3-161-2003, 2003.
- 810 Shi, Z. B., Vu, T., Kotthaus, S., Harrison, R. M., Grimmond, S., Yue, S., Zhu, T., Lee, J., Han, Y., Demuzere, M., Dunmore, R. E., Ren, L. J., Liu, D., Wang, Y. L., Wild, O., Allan, J., Acton, W. J., Barlow, J., Barratt, B., Beddows, D., Bloss, W. J., Calzolari, G., Carruthers, D., Carslaw, D. C., Chan, Q., Chatzidiakou, L., Chen, Y., Crilley, L., Coe, H., Dai, T., Doherty, R., Duan, F., Fu, P., Ge, B., Ge, M., Guan, D., Hamilton, J. F., He, K., Heal, M., Heard, D., Hewitt, C. N., Holloway, M., Hu, M., Ji, D., Jiang, X. J., Jones, R., Kalberer, M., Kelly, F. J., Kramer, L., Langford, B., Lin, C., Lewis, A. C., Li, J., Li, W.,  
815 Liu, H., Liu, J. F., Loh, M., Lu, K. D., Lucarelli, F., Mann, G., McFiggans, G., Miller, M. R., Mills, G., Monk, P., Nemitz, E., O'Connor, F., Bin O. u. y. a. n. g. , Palmer, P. I., Percival, C., Popoola, O., Reeves, C., Rickard, A. R., Shao, L. Y., Shi, G. Y., Spracklen, D., Stevenson, D., Sun, Y., Sun, Z. W., Tao, S., Tong, S. R., Wang, Q. Q., Wang, W. H., Wang, X. M., Wang, X. J., Wang, Z. F., Wei, L. F., Whalley, L., Wu, X. F., Wu, Z. J., Xie, P. H., Yang, F. M., Zhang, Q., Zhang, Y. L., Zhang, Y. H., and Zheng, M.: Introduction to the special issue "In-depth study of air pollution sources and processes within  
820 Beijing and its surrounding region (APHH-Beijing)", *Atmos Chem Phys*, 19, 7519-7546, 10.5194/acp-19-7519-2019, 2019.
- Slater, E. J., Whalley, L. K., Woodward-Massey, R., Ye, C., Lee, J. D., Squires, F. A., Hopkins, J., Dunmore, R., Shaw, M., Hamilton, J. F., Lewis, A. C., Crilley, L., Kramer, L., Bloss, W. J., Vu, T., Sun, Y., Xu, W., Yue, S., Ren, L., Acton, W. J., Hewitt, C. N., Wang, X., Fu, P., and Heard, D. E.: Elevated levels of OH observed in haze events during wintertime in central Beijing, *Atmospheric Chemistry and Physics Discussions*, 362, 2020.
- 825 Squires, F. A., Nemitz, E., Langford, B., Wild, O., Drysdale, W. S., Acton, W. J., Fu, P., Grimmond, C. S. B., Hamilton, J. F., Hewitt, C. N., Holloway, M., Kotthaus, S., Lee, J., Metzger, S., Pingingtha-Durden, N., Shaw, M., Vaughan, A. R., Wang, X., Wu, R., Zhang, Q., and Zhang, Y.: Measurements of traffic-dominated pollutant emissions in a Chinese megacity, *Atmos Chem Phys*, 20, 8737-8761, 2020.
- Tan, Z. F., Fuchs, H., Lu, K. D., Hofzumahaus, A., Bohn, B., Broch, S., Dong, H. B., Gomm, S., Haseler, R., He, L. Y.,  
830 Holland, F., Li, X., Liu, Y., Lu, S. H., Rohrer, F., Shao, M., Wang, B. L., Wang, M., Wu, Y. S., Zeng, L. M., Zhang, Y. S.,



- Wahner, A., and Zhang, Y. H.: Radical chemistry at a rural site (Wangdu) in the North China Plain: observation and model calculations of OH, HO<sub>2</sub> and RO<sub>2</sub> radicals, *Atmos Chem Phys*, 17, 663-690, 10.5194/acp-17-663-2017, 2017.
- Tan, Z. F., Lu, K. D., Hofzumahaus, A., Fuchs, H., Bohn, B., Holland, F., Liu, Y. H., Rohrer, F., Shao, M., Sun, K., Wu, Y. S., Zeng, L. M., Zhang, Y. S., Zou, Q., Kiendler-Scharr, A., Wahner, A., and Zhang, Y. H.: Experimental budgets of OH, HO<sub>2</sub>, and RO<sub>2</sub> radicals and implications for ozone formation in the Pearl River Delta in China 2014, *Atmos Chem Phys*, 19, 7129-7150, 10.5194/acp-19-7129-2019, 2019.
- Tan, Z. F., Hofzumahaus, A., Lu, K. D., Brown, S. S., Holland, F., Huey, L. G., Kiendler-Scharr, A., Li, X., Liu, X. X., Ma, N., Min, K. E., Rohrer, F., Shao, M., Wahner, A., Wang, Y. H., Wiedensohler, A., Wu, Y. S., Wu, Z. J., Zeng, L. M., Zhang, Y. H., and Fuchs, H.: No Evidence for a Significant Impact of Heterogeneous Chemistry on Radical Concentrations in the North China Plain in Summer 2014, *Environ Sci Technol*, 54, 5973-5979, 10.1021/acs.est.0c00525, 2020.
- Wang, S. N., Wu, R. R., Berndt, T., Ehn, M., and Wang, L. M.: Formation of Highly Oxidized Radicals and Multifunctional Products from the Atmospheric Oxidation of Alkylbenzenes, *Environ Sci Technol*, 51, 8442-8449, 10.1021/acs.est.7b02374, 2017b.
- Wang, T., Ding, A. J., Gao, J., and Wu, W. S.: Strong ozone production in urban plumes from Beijing, China, *Geophys Res Lett*, 33, Artn L21806 10.1029/2006gl027689, 2006.
- Wang, T., Nie, W., Gao, J., Xue, L. K., Gao, X. M., Wang, X. F., Qiu, J., Poon, C. N., Meinardi, S., Blake, D., Wang, S. L., Ding, A. J., Chai, F. H., Zhang, Q. Z., and Wang, W. X.: Air quality during the 2008 Beijing Olympics: secondary pollutants and regional impact, *Atmos Chem Phys*, 10, 7603-7615, 10.5194/acp-10-7603-2010, 2010.
- Wang, T., Xue, L. K., Brimblecombe, P., Lam, Y. F., Li, L., and Zhang, L.: Ozone pollution in China: A review of concentrations, meteorological influences, chemical precursors, and effects, *Sci Total Environ*, 575, 1582-1596, 10.1016/j.scitotenv.2016.10.081, 2017a.
- Whalley, L. K., Edwards, P. M., Furneaux, K. L., Goddard, A., Ingham, T., Evans, M. J., Stone, D., Hopkins, J. R., Jones, C. E., Karunaharan, A., Lee, J. D., Lewis, A. C., Monks, P. S., Moller, S. J., and Heard, D. E.: Quantifying the magnitude of a missing hydroxyl radical source in a tropical rainforest, *Atmos Chem Phys*, 11, 7223-7233, 10.5194/acp-11-7223-2011, 2011.
- Whalley, L. K., Blitz, M. A., Desservettaz, M., Seakins, P. W., and Heard, D. E.: Reporting the sensitivity of laser-induced fluorescence instruments used for HO<sub>2</sub> detection to an interference from RO<sub>2</sub> radicals and introducing a novel approach that enables HO<sub>2</sub> and certain RO<sub>2</sub> types to be selectively measured, *Atmos Meas Tech*, 6, 3425-3440, 10.5194/amt-6-3425-2013, 2013.
- Whalley, L. K., Stone, D., Bandy, B., Dunmore, R., Hamilton, J. F., Hopkins, J., Lee, J. D., Lewis, A. C., and Heard, D. E.: Atmospheric OH reactivity in central London: observations, model predictions and estimates of in situ ozone production, *Atmos Chem Phys*, 16, 2109-2122, 10.5194/acp-16-2109-2016, 2016.
- Whalley, L. K., Stone, D., Dunmore, R., Hamilton, J., Hopkins, J. R., Lee, J. D., Lewis, A. C., Williams, P., Kleffmann, J., Laufs, S., Woodward-Massey, R., and Heard, D. E.: Understanding in situ ozone production in the summertime through



- 865 radical observations and modelling studies during the Clean air for London project (ClearfLo), *Atmos Chem Phys*, 18, 2547-  
2571, 10.5194/acp-18-2547-2018, 2018.
- Woodward-Massey, R., Slater, E. J., Alen, J., Ingham, T., Cryer, D. R., Stimpson, L. M., Ye, C. X., Seakins, P. W., Whalley,  
L. K., and Heard, D. E.: Implementation of a chemical background method for atmospheric OH measurements by laser-  
induced fluorescence: characterisation and observations from the UK and China, *Atmos Meas Tech*, 13, 3119-3146,  
870 10.5194/amt-13-3119-2020, 2020.
- Xue, L. K., Saunders, S. M., Wang, T., Gao, R., Wang, X. F., Zhang, Q. Z., and Wang, W. X.: Development of a chlorine  
chemistry module for the Master Chemical Mechanism, *Geosci Model Dev*, 8, 3151-3162, 10.5194/gmd-8-3151-2015, 2015.
- Zhou, W., Zhao, J., Ouyang, B., Mehra, A., Xu, W. Q., Wang, Y. Y., Bannan, T. J., Worrall, S. D., Priestley, M., Bacak, A.,  
Chen, Q., Xie, C. H., Wang, Q. Q., Wang, J. F., Du, W., Zhang, Y. J., Ge, X. L., Ye, P. L., Lee, J. D., Fu, P. Q., Wang, Z. F.,  
875 Worsnop, D., Jones, R., Percival, C. J., Coe, H., and Sun, Y. L.: Production of N<sub>2</sub>O<sub>5</sub> and ClNO<sub>2</sub> in summer in urban  
Beijing, China, *Atmos Chem Phys*, 18, 11581-11597, 10.5194/acp-18-11581-2018, 2018.

880



**Table 1: Chemical reactions that were used in the experimental budget analysis for OH, HO<sub>2</sub>, RO<sub>2</sub> and RO<sub>x</sub>. The rate coefficient at 298K are given in column 3; temperature dependent rate coefficients were used in the experimental budget analysis presented in section 3.3**

No.	Reaction	Rate coefficient (298K) cm <sup>3</sup> molecule <sup>-1</sup> s <sup>-1</sup>
<b>R1</b>	Alkene + O <sub>3</sub> → OH, HO <sub>2</sub> , RO <sub>2</sub> + products	Specific rate coefficients and radical yields for each alkene, taken from the MCM3.3.1 (Jenkin et al., 2015)
<b>R2</b>	NO + HO <sub>2</sub> → OH + NO	8.5 × 10 <sup>-12</sup>
<b>R3</b>	O <sub>3</sub> + HO <sub>2</sub> → OH + 2O <sub>2</sub>	2.0 × 10 <sup>-15</sup>
<b>R4</b>	HCHO + OH + O <sub>2</sub> → CO + HO <sub>2</sub> + H <sub>2</sub> O	8.4 × 10 <sup>-12</sup>
<b>R5</b>	CO + OH + O <sub>2</sub> → HO <sub>2</sub> + CO <sub>2</sub>	2.3 × 10 <sup>-13</sup>
<b>R6</b>	RO <sub>2</sub> + NO → RO + NO <sub>2</sub>	8.7 × 10 <sup>-12</sup>
<b>R7</b>	HO <sub>2</sub> + NO → OH + NO <sub>2</sub>	8.5 × 10 <sup>-12</sup>
<b>R8</b>	HO <sub>2</sub> + O <sub>3</sub> → OH + 2O <sub>2</sub>	2.0 × 10 <sup>-15</sup>
<b>R9</b>	HO <sub>2</sub> + RO <sub>2</sub> → ROOH + O <sub>2</sub>	2.3 × 10 <sup>-11</sup>
<b>R10</b>	HO <sub>2</sub> + HO <sub>2</sub> → H <sub>2</sub> O <sub>2</sub> + O <sub>2</sub>	1.7 × 10 <sup>-12</sup>
	HO <sub>2</sub> + HO <sub>2</sub> + H <sub>2</sub> O → H <sub>2</sub> O <sub>2</sub> + H <sub>2</sub> O + O <sub>2</sub>	6.4 × 10 <sup>-30</sup>
<b>R11</b>	RO <sub>2</sub> + RO <sub>2</sub> → products	3.5 × 10 <sup>-13</sup>
<b>R12</b>	OH + NO <sub>2</sub> → HNO <sub>3</sub>	1.1 × 10 <sup>-11</sup>
<b>R13</b>	OH + NO → HONO	7.5 × 10 <sup>-12</sup>



**Table 2: The species measured by DC-GC-FID and PTR-ToF-MS that have been used as constraints in the model**

<b>Instrument</b>	<b>Species</b>	<b>Reference</b>
DC-GC_FID	CH <sub>4</sub> , C <sub>2</sub> H <sub>6</sub> , C <sub>2</sub> H <sub>4</sub> , C <sub>3</sub> H <sub>8</sub> , C <sub>3</sub> H <sub>6</sub> , isobutane, butane, C <sub>2</sub> H <sub>2</sub> , trans-but-2-ene, but-1-ene, Isobutene, cis-but-2-ene, 2-Methylbutane, pentane, 1,3-butadiene, trans-2-pentene, cis-2-pentene, 2-methylpentane, 3-methylpentane, hexane, isoprene, heptane, Benzene, Toluene, o-xylene, CH <sub>3</sub> OH, CH <sub>3</sub> OCH <sub>3</sub> , ethylbenzene, CH <sub>3</sub> CHO, C <sub>2</sub> H <sub>5</sub> OH	Hopkins et al. (2011)
PTR-ToF-MS	$\alpha$ -pinene, limonene, isopropylbenzene, propylbenzene, xylene, trimethylbenzene.	Huang et al. (2016)



**Table 3: Different model scenarios that are discussed in section 3**

Model Name	Description
<b>Base model</b>	As described in section 2.4
<b>Base model-SA</b>	The base model with the inclusion of a first order loss process of HO <sub>2</sub> to aerosols calculated using Eq 9 with an uptake coefficient, $\gamma = 0.2$
<b>Base model-Cl</b>	The base model with the inclusion of Cl atom chemistry, taken from (Xue et al., 2015)
<b>Missing k(OH) (OH to CH<sub>3</sub>O<sub>2</sub>)</b>	The base model with an additional reaction converting OH to CH <sub>3</sub> O <sub>2</sub> at a rate equal to the missing reactivity
<b>Missing k(OH) (OH to HOCH<sub>2</sub>CH<sub>2</sub>O<sub>2</sub>)</b>	The base model with an additional reaction converting OH to HOCH <sub>2</sub> CH <sub>2</sub> O <sub>2</sub> at a rate equal to the missing reactivity
<b>Missing k(OH) (OH to CH<sub>3</sub>C(O)O<sub>2</sub>)</b>	The base model with an additional reaction converting OH to CH <sub>3</sub> C(O)O <sub>2</sub> at a rate equal to the missing reactivity
<b>Missing k(OH) (OH to C96O2)</b>  <b>C96O2 =</b> 	The base model with an additional reaction converting OH to C96O2 (which is an $\alpha$ -pinene derived RO <sub>2</sub> species) at a rate equal to the missing reactivity

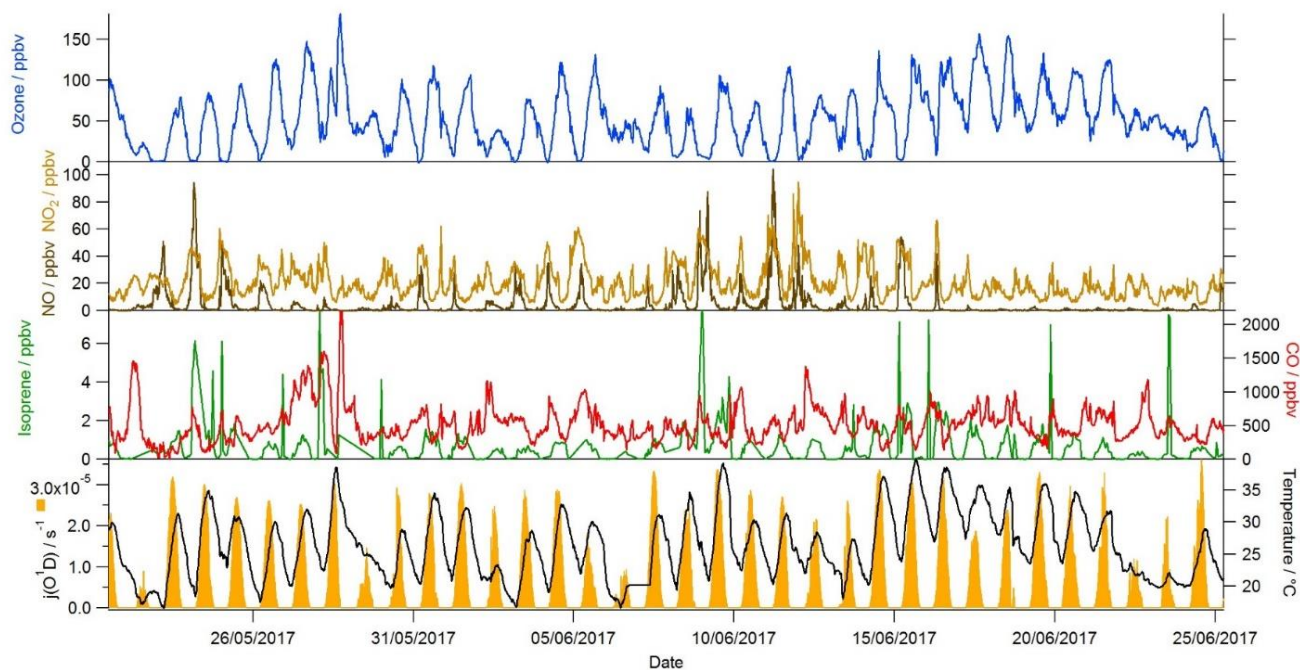


Figure 1: Time-series of ozone, NO, NO<sub>2</sub> isoprene, CO, j(O<sup>1</sup>D) and temperature during the campaign

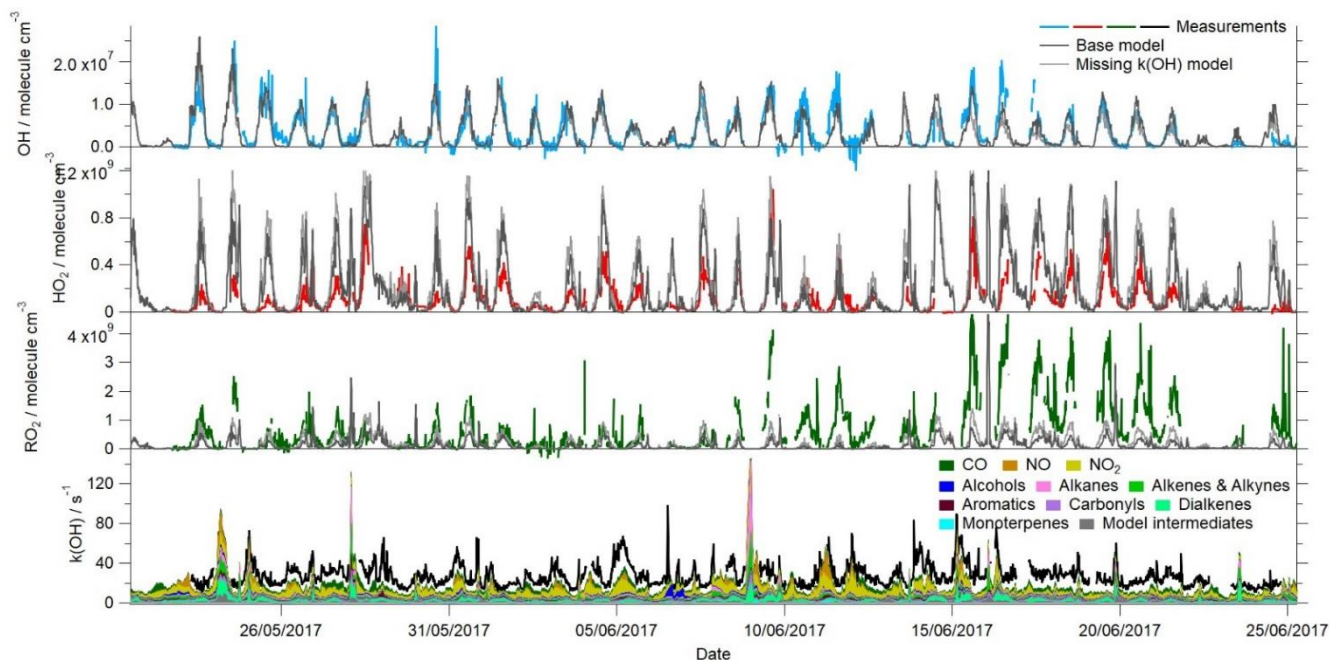
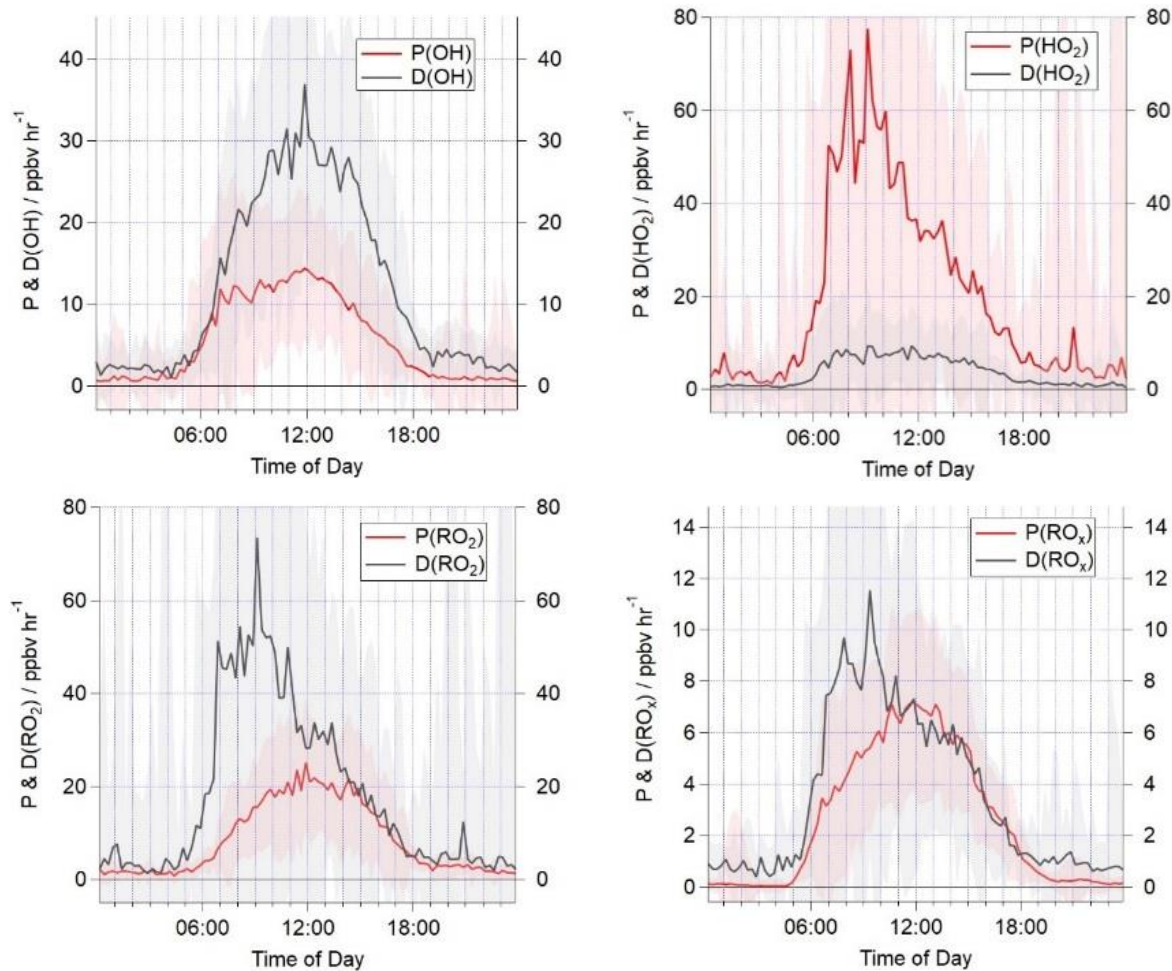


Figure 2: Time-series of the measured and modelled OH, HO<sub>2</sub>, total RO<sub>2</sub> and OH reactivity during the campaign



**Figure 3:** Campaign median production and destruction rates for OH, HO<sub>2</sub>, total RO<sub>2</sub> and RO<sub>x</sub>. The shaded areas represent the 1 $\sigma$  standard deviation of the data representing the variability from day to day

925

930

935

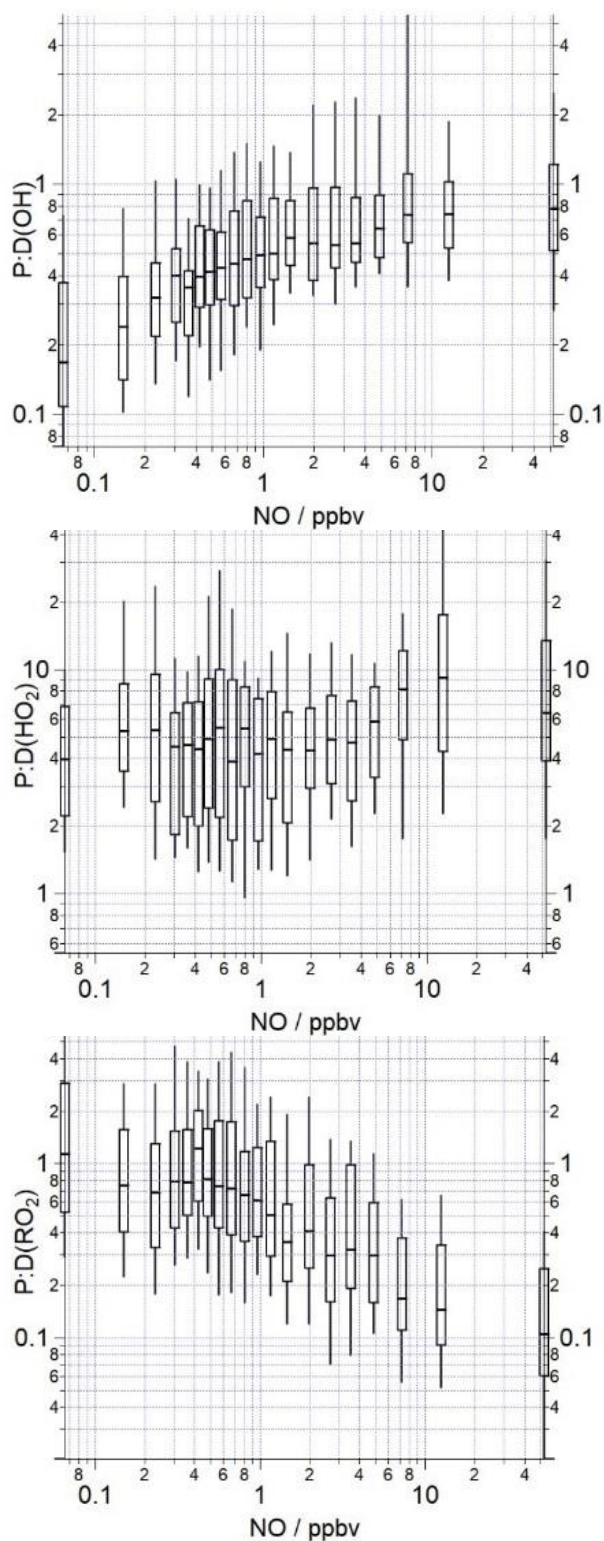
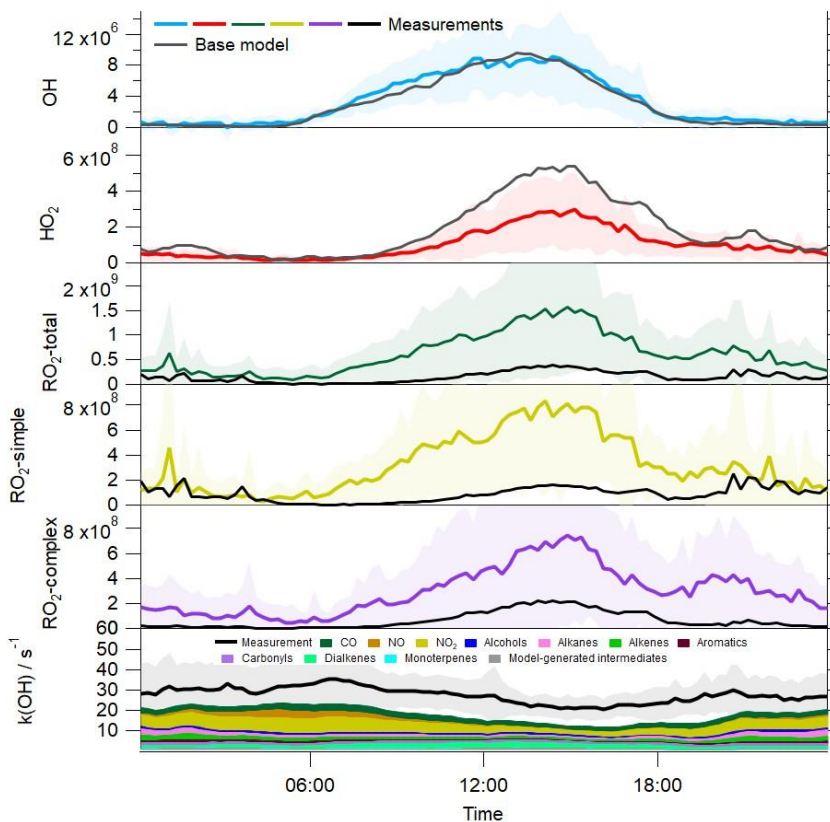


**Figure 4:** The median ratio of the OH, HO<sub>2</sub> and total RO<sub>2</sub> production rates to destruction rates binned over the NO mixing ratio range encountered during the campaign on a logarithmic scale. The box and whiskers represent the 25<sup>th</sup>/75<sup>th</sup> and 5<sup>th</sup>/95<sup>th</sup> confidence intervals. The number of data points in each of the NO bins is ~80



990 **Figure 5: Average profiles for the observed OH, HO<sub>2</sub>, total RO<sub>2</sub>, partially-speciated RO<sub>2</sub> (in molecule cm<sup>-3</sup>) and OH reactivity at 15 minute intervals over 24 hours. The error bars represent the 1  $\sigma$  standard deviation of the measurements representing the variability in the measurements from day to day. The average diurnal profiles for OH, HO<sub>2</sub>, total RO<sub>2</sub>, partially speciated RO<sub>2</sub> and OH reactivity from the base model are overlaid**

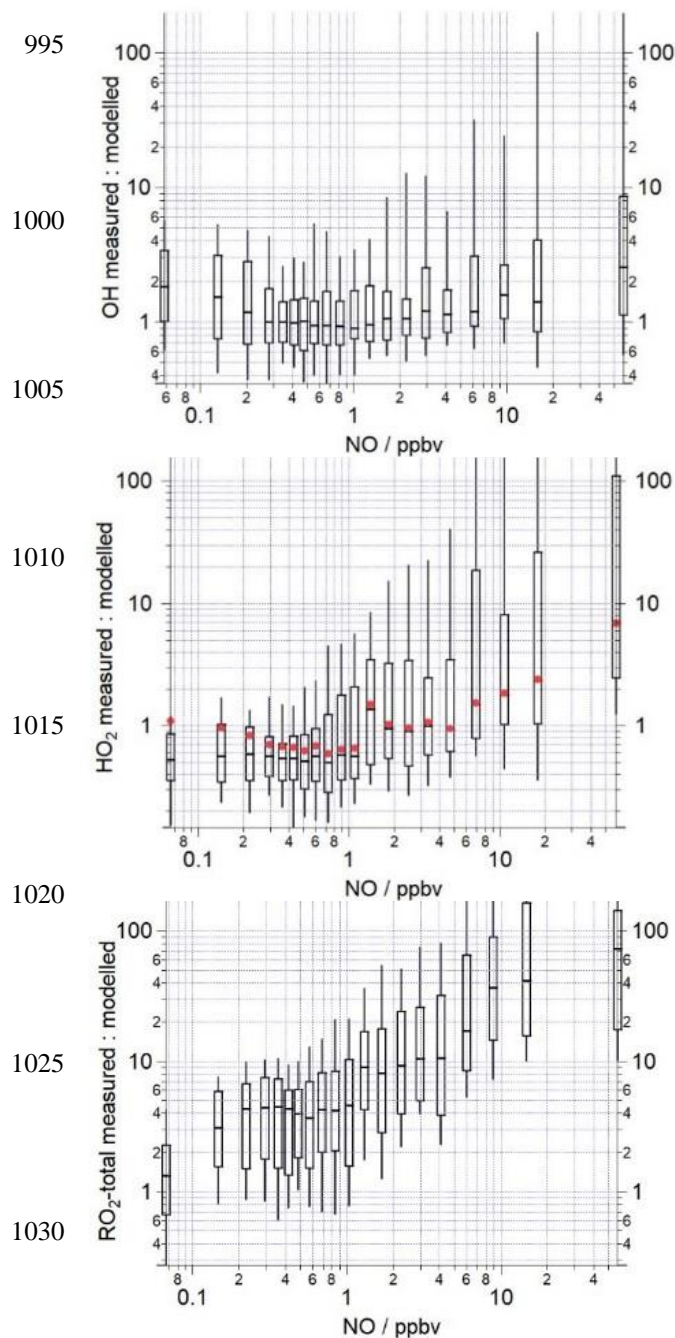
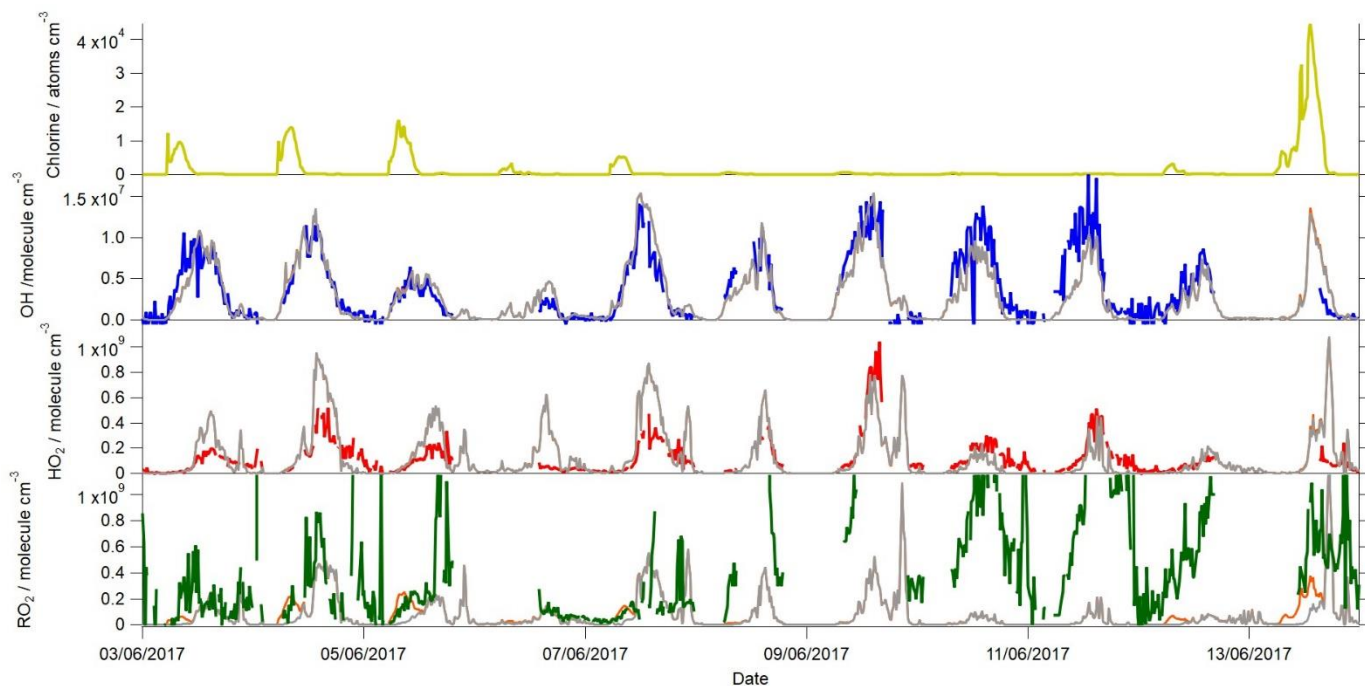


Figure 6: The median ratio (-) of the measured to modelled OH, HO<sub>2</sub> and total RO<sub>2</sub> binned over the NO mixing ratio range encountered during the campaign on a logarithmic scale. The box and whiskers represent the 25<sup>th</sup>/75<sup>th</sup> and 5<sup>th</sup>/95<sup>th</sup> confidence intervals. The red circles in the middle panel display the measured to modelled HO<sub>2</sub> ratio when the model includes a heterogeneous loss of HO<sub>2</sub> to aerosols calculated using Eq. 9. The number of data points in each of the NO bins is ~80

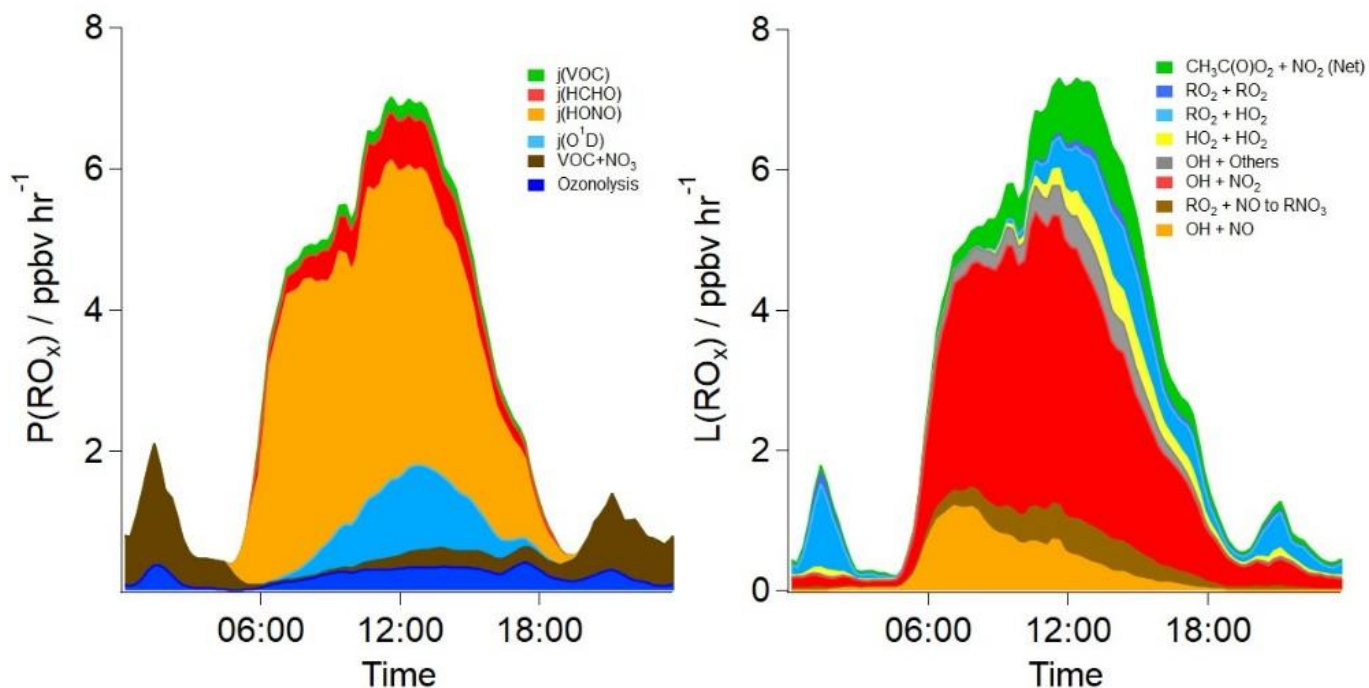


1040



**Figure 7: Time-series of the measured and modelled OH, HO<sub>2</sub>, total RO<sub>2</sub> during the campaign when ClNO<sub>2</sub> was also measured. The Cl atom concentration calculated to be present is shown in the top panel. The measured OH concentrations are represented by the blue line, HO<sub>2</sub> by the red line and total RO<sub>2</sub> by the green line. The base model scenario is shown in grey, whilst the base model with Cl atom chemistry included (Xue et al., 2015) is shown in orange**

1045



1050 **Figure 8: The average diurnal rates of primary production and termination for RO<sub>x</sub> radicals in ppbv hr<sup>-1</sup> in the base model scenario. CH<sub>3</sub>C(O)O<sub>2</sub> + NO<sub>2</sub> (Net) represents the net rate (forward minus backward) for all RC(O)O<sub>2</sub> + NO<sub>2</sub> ↔ PAN species**

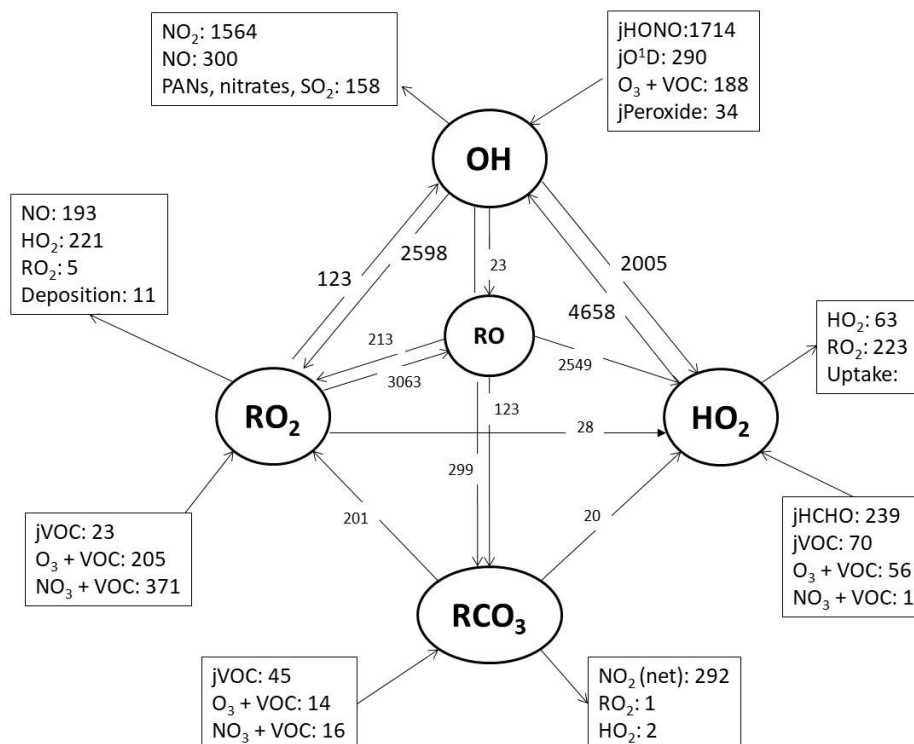
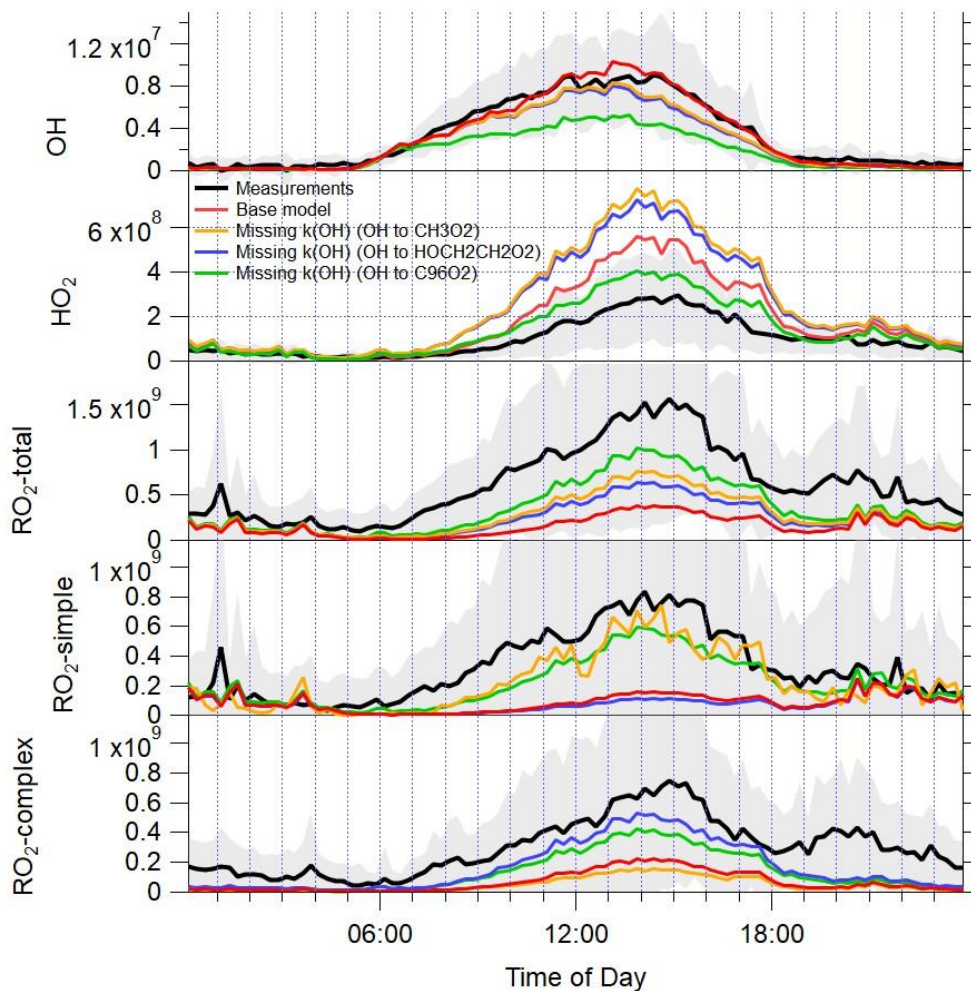
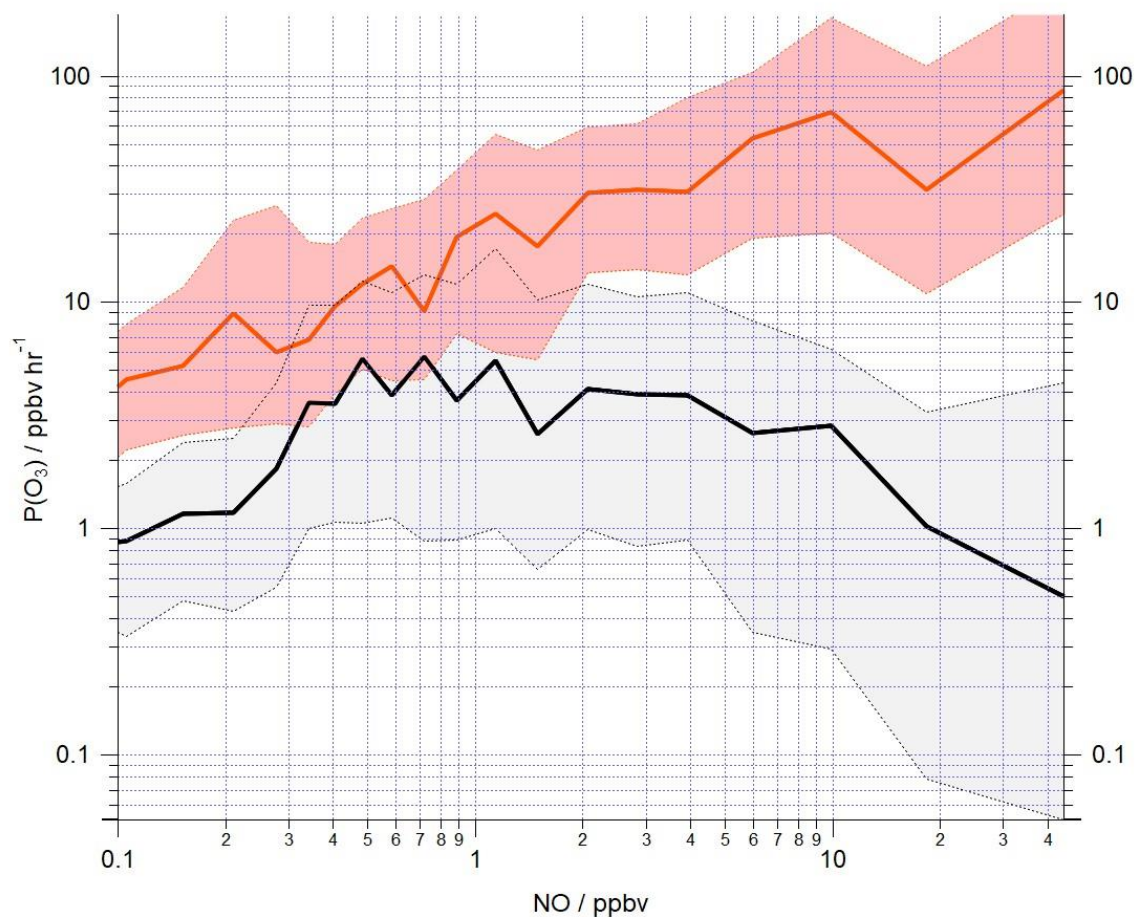


**Figure 9: A model reaction flux analysis, showing the mean rate of reaction for formation, propagation and termination of radicals (ppty hr<sup>-1</sup>) (day and night) during the whole campaign**

1055



1060 **Figure 10:** Average diel profiles for the observed OH, HO<sub>2</sub>, total RO<sub>2</sub>, and partially-speciated RO<sub>2</sub> (black lines) at 15 minute intervals over 24 hours. The error bars represent the 1  $\sigma$  standard deviation of the measurements. The average OH, HO<sub>2</sub>, total RO<sub>2</sub> and partially speciated RO<sub>2</sub> model profiles when the missing reactivity observed at a given time is accounted for by different OH to RO<sub>2</sub> reactions are overlaid (yellow, blue and green lines); the base model predictions are in red. See text for details



1065 **Figure 11: Mean ozone production ( $\text{ppbv hr}^{-1}$ ) calculated from observed (red line) and modelled (black line)  $\text{RO}_x$  concentrations using Eq. (11) binned over the NO mixing ratio range encountered during the campaign on a logarithmic scale. The shading represents the 25<sup>th</sup> / 75<sup>th</sup> percentile confidence limits. The number of data points in each of the NO bins is ~80**

1070